A quantitative explanation of the observed population of Milky Way satellite galaxies

Draft version October 24, 2018
Preprint typeset using LaTeX style emulateapj v. 04/20/08

A QUANTITATIVE EXPLANATION OF THE OBSERVED POPULATION OF MILKY WAY SATELLITE GALAXIES.

Sergey E. Koposov[1,2,3], Jaiyul Yoo[4], Hans-Walter Rix[1], David H. Weinberg[5], Andrea V. Macciò[1], Jordi Miralda-Escudé[6],

Draft version October 24, 2018

ABSTRACT

We revisit the well known discrepancy between the observed number of Milky Way (MW) dwarf satellite companions and the predicted population of cold dark matter (CDM) sub-halos, in light of the dozen new low luminosity satellites found in imaging data from the Sloan Digital Sky Survey (SDSS) and our recent calibration of the SDSS satellite detection efficiency, which implies a total satellite population far larger than these dozen discoveries. We combine a detailed dynamical model for the CDM sub-halo population with simple, physically motivated prescriptions for assigning a stellar content to each sub-halo, then apply observational selection effects and compare to the current observational census. Reconciling the observed satellite population with CDM predictions still requires strong mass-dependent suppression of star formation in low mass sub-halos: models in which the stellar mass is a constant fraction $F_*(\Omega_b/\Omega_m)$ of the sub-halo mass $M_{\rm sat}$ at the time it becomes a satellite fail for any choice of F_*. However, previously advocated models that invoke suppression of gas accretion after reionization in halos with circular velocity $V_{\rm circ} \leq V_{\rm crit} \approx 35\,{\rm km\ s^{-1}}$ can reproduce the observed satellite counts for $-15 \leq M_V \leq 0$. Successful models require $F_* \approx 10^{-3}$ in halos with $V_{\rm circ} > V_{\rm crit}$ and strong suppression of star formation *before* reionization in halos with $V_{\rm circ} \lesssim 10\,{\rm km\ s^{-1}}$; models without pre-reionization suppression predict far too many satellites with $-5 \leq M_V \leq 0$. In this successful model, the dominant fraction of stars formed after reionization at all luminosities. Models that match the satellite luminosity distribution also match the observed heliocentric radius distribution, and they reproduce the observed characteristic stellar velocity dispersion $\sigma_* \approx 5-10\,{\rm km\ s^{-1}}$ of the SDSS dwarfs given the observed sizes ($\sim 50-200\,{\rm pc}$) of their stellar distributions. The model satellites have $M(<300\,{\rm pc}) \sim 10^7 M_\odot$ as observed even though their present day total halo masses span more than two orders of magnitude; the constancy of central masses mainly reflects the profiles of CDM halos. Our modeling shows that natural physical mechanisms acting within the CDM framework can quantitatively explain the properties of the MW satellite population as it is presently known, thus providing a convincing solution to the 'missing satellite' problem.

Subject headings: Galaxy: halo – Galaxy: structure – Galaxy: formation – Local Group

1. INTRODUCTION

The inflationary cold dark matter scenario predicts an initial fluctuation spectrum with power that continues down to small scales, and in consequence it predicts a mass function of dark matter halos that rises steeply towards low masses. A significant fraction of these halos survive as gravitationally self-bound units long after falling into more massive halos. As pointed out forcefully by Klypin et al. (1999) and Moore et al. (1999), the predicted number of sub-halos within a Milky Way-like galaxy halo greatly exceeded the then known numbers of Milky Way or Local Group dwarf satellites, when sub-halos and observed dwarfs were matched based on velocity dispersion or corresponding circular velocity (see also Kauffmann et al. 1993). This discrepancy between predicted and observed numbers has become known as the "missing satellite problem."

Proposed solutions fall into three general categories. The first modifies the properties of dark matter or the primordial fluctuations from inflation in a way that eliminates the low mass dark matter sub-halos themselves (e.g. Kamionkowski & Liddle 2000; Spergel & Steinhardt 2000; Bode et al. 2001; Zentner & Bullock 2003). The second appeals to astrophysical mechanisms that suppress star formation in low mass halos so that they do not become observable dwarf satellites; photo-heating by the meta-galactic UV background is an attractive mechanism because it naturally introduces a cutoff at approximately the correct velocity scale (Bullock et al. 2000; Somerville 2002; Kravtsov et al. 2004). The third possibility, arguably a variant of the second, is that the numerous dwarf companions of the Milky Way actually exist but have been missed by observational searches.

In this paper we revisit the "missing satellite problem" with particular emphasis on the role of the new dwarf companions discovered in imaging data from the Sloan Digital Sky Survey (SDSS; York et al. 2000;

[1] Max Planck Institute for Astronomy, Königstuhl 17, 69117 Heidelberg, Germany;
[2] Institute of Astronomy, University of Cambridge, Madingley Road, Cambridge, UK
[3] Sternberg Astronomical Institute, Universitetskiy pr. 13, 119992 Moscow, Russia
[4] Harvard-Smithsonian Center for Astrophysics, Harvard University, 60 Garden Street, Cambridge, MA 02138
[5] Ohio State University, Department of Astronomy and CCAPP, Columbus, OH 43210, USA
[6] Institució Catalana per la Recerca i Estudis Avançats, Barcelona, Spain / Institut de Ciències del Cosmos, Universitat de Barcelona, Spain

Adelman-McCarthy et al. 2008). There are now about a dozen of these (Willman et al. 2005; Belokurov et al. 2006, 2007; Zucker et al. 2006; Irwin et al. 2007; Koposov et al. 2007; Walsh et al. 2007; a couple of systems still have ambiguous status), most of them at least an order of magnitude less luminous than the faintest of the previously known, "classical" satellites.[7] Spectroscopic follow-up (e.g. Martin et al. 2007; Simon & Geha 2007; Geha et al. 2008) for many of them indicates that they are indeed dark matter dominated systems, even though most are fainter than typical globular clusters, as low as only $\sim$1000 $L_\odot$ (e.g. Belokurov et al. 2007; Martin et al. 2008). Remarkably, almost all of the newly found faint satellite galaxies have stellar velocity dispersions in the range $3 - 10\,\mathrm{km\ s^{-1}}$, though their luminosities vary widely. Similarly, the total masses within the inner 300 pc span less than an order of magnitude (Strigari et al. 2008).

Since the SDSS imaging in which these satellites have been discovered covers only $\sim 20\%$ of the sky, a naive accounting would increase the estimated number of Milky Way companions by $5 \times 12 = 60$, in addition to the ten classical satellites. However, Koposov et al. (2008) use a well-defined identification algorithm to show that the SDSS dwarfs are also subject to strong radial selection effects. Most of the newly discovered objects could only have been found within distances of 50-100 kpc, much smaller than the inferred virial radius of the Milky Way's dark matter halo (~ 280 kpc for $\rho_{\rm vir}/\bar{\rho} = 340$; Xue et al. 2008). The faintest SDSS dwarfs are detectable over only 1/1000 of the halo virial volume (including the factor of five for sky coverage). Walsh et al. (2008) have recently reached similar conclusions based on an independent identification algorithm and independent Monte Carlo tests.

Such analyses are the basis for 'volume corrections' for the faint Milky Way satellite population. With proper volume corrections applied, the luminosity function of faint Milky Way satellite galaxies turns out to be a rather shallow power law in the range $-15 < M_V < -3$ (Koposov et al. 2008). These results in turn imply that the number of satellites brighter than $M_V = -3$ is $\sim$ 80 or more, and the number above $M_V = 0$ could be a few hundred. Tollerud et al. (2008) reached a similar conclusion, adopting a radial satellite distribution based on the *Via Lactea* simulation of Diemand et al. (2007). Even this census counts only dwarfs that are above the effective surface brightness threshold for SDSS detection. With the Koposov et al. (2008) detection algorithm, this threshold is approximately 30 mag arcsec^{-2} (V-band), with a weak dependence on luminosity and distance. The dwarfs found in SDSS have surface brightnesses that range from 24 to 30 mag arcsec^{-2}.

Studies of the high redshift Lyα forest indicate that the small scale power expected in the standard ΛCDM scenario (inflationary cold dark matter with a cosmological constant) is indeed present in the primordial fluctuation spectrum (Narayanan et al. 2000; Viel et al. 2005; Abazajian 2006; Seljak et al. 2006). Astrophysical suppression of star formation, and photo-ionization suppression in particular, has emerged as the most plausible and hence popular solution to the "missing satellite" conundrum. Within this category, there have been different proposals about what sub-halos host the observed dwarf satellites. Bullock et al. (2000) suggested that the observed dwarfs are those whose sub-halos assembled a substantial fraction of their mass before reionization, and thus before the onset of photo-ionization suppression. Stoehr et al. (2002) suggested that the measured stellar velocity dispersions are well below the virial velocity dispersions of the dark matter sub-halos, and that the observed dwarfs occupy sub-halos that are still above the velocity threshold where star-formation suppression occurs. Kravtsov et al. (2004) used N-body simulations to show that roughly 10% of sub-halos lose a large fraction ($\sim 90\%$) of their mass during dynamical evolution without being completely disrupted; they suggested that the observed dwarfs occupy sub-halos that were above the suppression threshold at the time they became satellites but have suffered extensive mass loss since then. These papers and others (e.g., Somerville 2002; Strigari et al. 2007; Orban et al. 2008) focus on explaining the classical (pre-SDSS) dwarf spheroidal population, with luminosities in the range $-8 < M_V < -15$ (excluding the Magellanic clouds) and stellar velocity dispersions in the range $8\,\mathrm{km\ s^{-1}} < \sigma_* < 25\,\mathrm{km\ s^{-1}}$. The recently discovered SDSS dwarfs have much lower luminosities ($-8 < M_V < -1.5$), lower surface brightness, and somewhat lower velocity dispersion ($\sigma_* \sim 5\,\mathrm{km\ s^{-1}}$), so they could have a distinct formation mechanism, or they could form a continuum with the classical dwarf spheroidals.

The new SDSS discoveries and their quantified detectability are the basis for the model-data comparison in this paper. We construct and test models of the Milky Way dwarf satellite population that incorporate Monte Carlo realizations of merger trees for $10^{12} M_\odot$ (main galaxy) halos, a detailed analytic model for the dynamical evolution and disruption of sub-halos, and a variety of recipes for assigning stellar masses to these sub-halos motivated by ideas in the existing literature. For most of our models, we assume that a sub-halo can only accrete gas to form stars (a) before the epoch of reionization or (b) after reionization if its virial velocity exceeds a critical threshold before it enters the Milky Way halo and becomes a satellite. The spirit of the exercise is similar to that of Bullock et al. (2000), but the dynamical modeling of sub-halos is more sophisticated, and we are now in a position to include directly the (strong) constraints imposed by the SDSS dwarfs accounting for the radial selection function found by Koposov et al. (2008). In contrast to most previous studies, we treat the luminosity distribution as the primary test of models, rather than the stellar velocity dispersions or central masses (Strigari et al. 2007, 2008; Li et al. 2008; Macciò et al. 2009), or the inferred but unobservable sub-halo circular velocities. This emphasis is motivated by the fact that the luminosity is the foremost quantity that matters for the observational selection. We consider stellar velocity dispersions and central masses as an additional test, but their interpretations are affected by the uncertainty in the dark matter profiles of the sub-halos associated with observed dwarfs.

2. THE POPULATION OF DARK MATTER SUB-HALOS IN THE MILKY WAY

[7] Throughout the paper we use "faint" and "bright" to refer to intrinsic luminosity rather than apparent brightness.

Our model for the Milky Way satellites is based on the cold dark matter scenario, with each satellite forming initially in a separate dark matter halo that at some point falls into the Milky Way's dark matter halo. We refer to the bound dark matter satellites orbiting in the Milky Way halo as sub-halos. A sub-halo may or may not correspond to a dwarf satellite galaxy, depending on whether it contains an observable number of stars. In this Section we describe our model for computing the dynamical evolution of sub-halos.

We use the dynamical dark-matter-only model of sub-halos developed by Yoo et al. (2007) to compute the sub-halo population and its orbital distribution. This model is described in detail in Yoo et al. (2007), where a much larger halo of $10^{15}\,M_\odot$ was considered as a model of a massive cluster of galaxies. Here we consider instead a final halo of $10^{12}\,M_\odot$ at the present time as a representation of the Milky Way galaxy. Despite the change in the final halo mass, the model remains basically the same as described in Yoo et al. (2007), so here we make only a brief summary of its description.

The model uses the extended Press-Schechter formalism to generate a Monte Carlo merger tree of the parent halo at the present time (Press & Schechter 1974; Bond et al. 1991). We follow the dynamical evolution of all the sub-halos with masses $M_h > 10^6\,M_\odot$ until they merge with the Milky Way and lose their mass below $M_h = 10^5\,M_\odot$. All halos start as isolated objects, and they grow in mass by accretion and mergers for as long as they remain isolated. At some redshift, $z_{\rm sat}$, they merge into a larger halo (either the Milky Way or another object that will become a Milky Way sub-halo). After this merger, the object has become a satellite or sub-halo and it stops growing in mass. It can subsequently lose mass by tidal stripping when it passes near the center of its parent halo or undergoes encounters with other sub-halos. The sub-halo is subject to dynamical friction, which tends to shrink its orbit, and to random encounters with other sub-halos, which on average expand the orbit. The orbital eccentricity is also subject to random variations. The model allows for the presence of sub-halos within other sub-halos. When a sub-halo is disrupted, any sub-halos it contained are dispersed into the new, larger parent halo. This simple analytic model is able to reproduce the sub-halo mass function, in reasonably good agreement with that found in numerical N-body simulations (Zentner et al. 2005; Shaw et al. 2006; Yoo et al. 2007). For the present purpose, this approach has the advantage (over N-body) of easily affording the required mass resolution and multiple halo realizations.

We adopt a flat ΛCDM cosmology with matter density $\Omega_m = 0.24$, baryon density $\Omega_b = 0.04$, power spectrum normalization $\sigma_8 = 0.8$, Hubble constant $h = 0.7$, and a primordial spectral index $n_s = 0.95$, consistent with recent measurements (Spergel et al. 2007; Tegmark et al. 2006). The matter power spectrum is computed by using the transfer function of Eisenstein & Hu (1999). We generate six Monte Carlo merger trees of a Milky-Way sized halo. Each realization provides the sub-halo mass function, their orbital elements and density profiles at the present time. Our statistical results are the average of the six different realizations.

The dynamical model of Yoo et al. (2007) uses the Jaffe profile and its velocity dispersion to model sub-halos and their dynamical interactions, for reasons of numerical simplicity and because large galaxies that are tidally-limited satellites of a larger halo are reasonably well modelled by a Jaffe sphere for their baryon plus dark matter density profiles. However, the very low-mass dwarf satellites tend to be dominated by dark matter even in their inner parts. We therefore make an adjustment to better connect our Monte Carlo simulation results to the observed Milky Way dwarf galaxies: we use the sub-halo masses and orbital elements, which are the quantities most robustly computed in the Yoo et al. (2007) model, but we calculate the density profiles and velocity dispersions of sub-halos assuming that they have an NFW profile (Navarro et al. 1997). Using the standard spherical collapse model, the virial radius of an isolated halo is assigned as

$$R_{\rm vir} = \left[\frac{3\,M_{\rm halo}}{4\,\pi\,\Delta_c\,\bar\rho_m(z)}\right]^{\frac{1}{3}}\,, \qquad (1)$$

where $\Delta_c = (18\,\pi^2 + 82\,x - 39\,x^2)/(1+x)$ (Bryan & Norman 1998), $x = -(1-\Omega_m)/(\Omega_m(1+z)^3 + 1 - \Omega_m)$, and the mean cosmic density is $\bar\rho_m(z) = \Omega_m\rho_c(1+z)^3$. The halo concentration c is computed using the relation from Bullock et al. (2001), scaled to $\sigma_8 = 0.8$ according to Macciò et al. (2007), with $c = 0.8\times 9\times\left(M_h/10^{13}h^{-1}M_\odot\right)^{-0.13}/(1+z)$.

For the model in this paper, we use in particular the sub-halo masses at two different special epochs: $M_{\rm rei} \equiv M_{\rm tot}(z = z_{\rm rei})$ when the universe reionizes and the photoionization background starts to suppress the star formation efficiency in low mass halos, and $M_{\rm sat} \equiv M_{\rm tot}(z_{\rm sat})$ at the epoch when a halo merges into a larger halo and we presume that subsequent star formation and gas accretion is halted in the sub-halo. We shall also use below the halo circular velocity $V_{\rm circ}$, which is the virial circular velocity, $V_{\rm circ} \equiv [(G\,M_{\rm tot})/R_{\rm vir}]^{1/2}$. (Here $M_{\rm tot}$ refers to the total mass including dark matter and a universal fraction of baryons.)

In Figure 1 we show the distribution of $\rm M_{sub-halo}$ at redshifts $z = 0$ (left panel), $z = z_{\rm sat}$ (middle panel) and $z = 8$, 11, and 14 (right panel). As expected, the mass distribution is close to a power-law, except near the resolution limit of our simulations. Also, in Figure 2 we show the accretion history of the MW sub-halo population, by plotting the halo masses of the present day MW sub-halos at the time of accretion vs. the redshift at which they became satellites of larger halos. We see that most of the MW sub-halos became satellites at $z < 2$. Most of the accreted satellites have small circular velocities $V_{\rm circ} < 20\,{\rm km\,s^{-1}}$, so they lie in a range where gas accretion and star formation are likely to be suppressed after the epoch of reionization (Quinn et al. 1996; Thoul & Weinberg 1996; Bullock et al. 2000).

3. POPULATING THE DM HALOS WITH STARS

3.1. *Recipes to assign stellar masses to sub-halos*

To make direct observational predictions from these models, we populate each sub-halo in a given Monte-Carlo realization with stars according to a sequence of recipes, then test how many of these satellites could have been found within the SDSS. Some of these recipes are

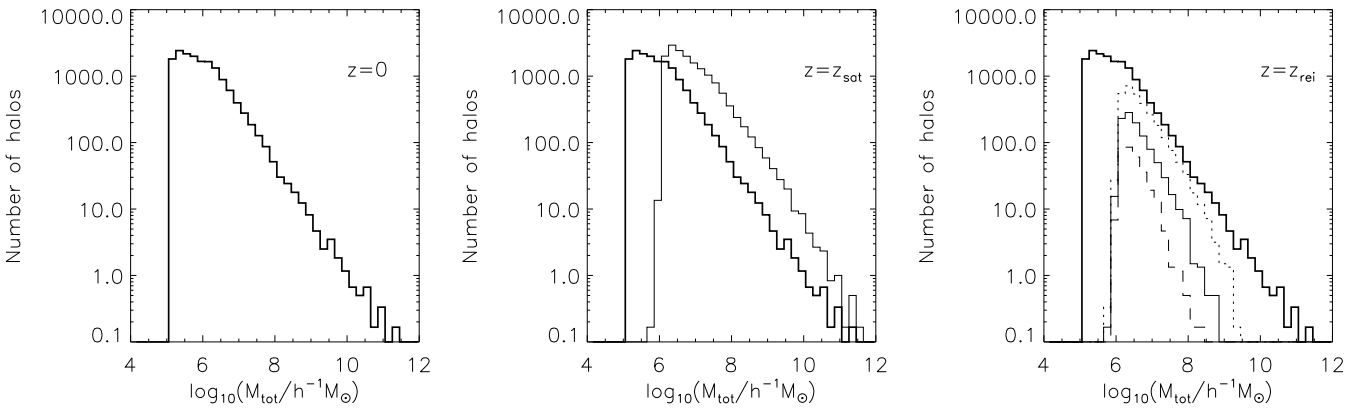

FIG. 1.— Mass distribution of dark matter sub-halos at different epochs. *Left panel*: The present-day ($z = 0$) mass function of sub-halos within a Milky Way-like halo. This histogram is repeated in the other two panels for reference. *Middle panel*: Distribution of mass that present-day sub-halos had at $z = z_{\rm sat}$, the epoch at which they became a satellite within a larger halo (*thin line*); tidal stripping of satellite halos is manifesting important. *Right panel*: Mass distribution of present day MW sub-halos at the epoch of reionization, for $z_{\rm rei} = 8$ (*dotted*), 11 (*thin solid*), and 14 (*dashed*). All panels reflect the average of six different realizations of MW-like halos. The flattening below $M = 10^6\,h^{-1}M_\odot$ and the sharp cut-off at $M = 10^5\,h^{-1}M_\odot$ arise from the mass resolution limits of our simulations.

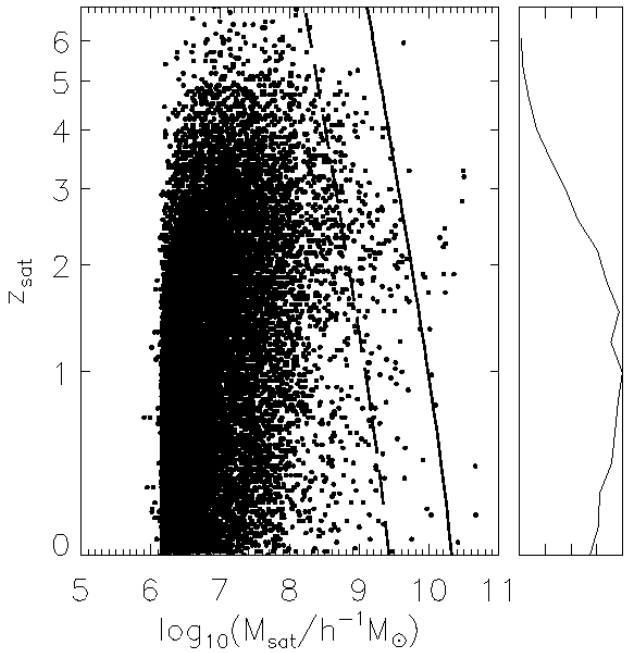

FIG. 2.— Epochs when (sub-)halos were accreted into larger halos, and masses at that time. This Figure illustrates the results from one Monte-Carlo realization of the semi-analytic model, with each point showing the redshift $z_{\rm sat}$ at which a sub-halo first became a satellite in a larger halo against its total mass $M_{\rm sat}$ at that epoch. The small panel on the right shows the distribution of $z_{\rm sat}$. Solid and dashed lines show the locus of halos with $V_{\rm circ}(z_{\rm sat}) = 40\,{\rm km\ s^{-1}}$ and $20\,{\rm km\ s^{-1}}$, respectively.

mathematically simple illustrations, while others are motivated by the expected effects of ionization and cooling physics as discussed in the introduction. For reference, the nomenclature of the recipes is summarized in Table 1. In all cases we calculate the stellar mass based on the sub-halo mass (dark matter plus baryons in the universal fraction) at the accretion epoch $z_{\rm sat}$, denoted $M_{\rm sat}$. We implicitly assume that satellites do not accrete new material to form additional stars and that tidal stripping of the dark matter does not affect the stellar content of the satellite if it survives to the present day. Simulations suggest that these assumptions are reasonable but not perfect approximations (Simha et al. 2008; Peñarrubia et al. 2008).

We begin with the simplest model (denoted Model 1A), that the stellar mass is a constant fraction of the sub-halo mass at the time of accretion into the main halo:

$$M_* = f_* \times M_{\rm sat}. \qquad (2)$$

The arguments of Klypin et al. (1999) and Moore et al. (1999) suggest that this model will fail badly, and we show that it does indeed fail despite the new satellite discoveries and the radial selection biases that affect them. There is ample evidence that the efficiency of star formation declines rapidly towards low masses even well above the dwarf satellite regime (e.g., van den Bosch et al. 2007). In Model 1B, we allow the stellar fraction to vary as a power law of $M_{\rm sat}$ below a threshold M_0:

$$M_* = f_* \times \mathtt{min}\left(\left(\frac{M_{\rm sat}}{M_0}\right)^{\alpha}, 1\right) \times M_{\rm sat}\ . \qquad (3)$$

Our second approach to modeling stellar masses includes the effects of a pervasive energetic radiation field after the epoch of reionization, which heats gas and hence keeps it from accumulating at the centers of low-mass halos. Calculations by Quinn et al. (1996) and Thoul & Weinberg (1996) showed that gas accretion in halos with the circular velocities below $V_{\rm circ} \sim 30 - 40\,{\rm km\ s^{-1}}$ is strongly suppressed, while substantially larger halos are minimally affected (see also Weinberg, Hernquist, & Katz 1997; Gnedin 2000). In this spirit, we assume that halos below a critical circular velocity form no stars after reionization, and we thus assign stellar masses

$$M_* = \begin{cases} f_* \times M_{\rm sat} & \text{if } V_{\rm circ}(z_{\rm sat}) > V_{\rm crit} \\ f_* \times M_{\rm rei} & \text{if } V_{\rm circ}(z_{\rm sat}) < V_{\rm crit}. \end{cases} \qquad (4)$$

This model (Model 2) has three adjustable parameters — f_*, $V_{\rm crit}$, and $z_{\rm rei}$ — with expectations that $V_{\rm crit} \sim 20 - 40\,{\rm km\ s^{-1}}$ and $z_{\rm rei} \sim 11$ (e.g. Weinmann et al. 2007;

Dunkley et al. 2008). The approach is similar to that of Bullock et al. (2000), except that we treat $V_{\rm crit}$ as free parameter, and the stellar mass formed before the epoch of reionization is assigned using $M_* = f_* \times M_{\rm rei}$, instead of simply dividing galaxies into "observable" or "unobservable" classes based on the fraction of the mass accreted by $z_{\rm rei}$.

Our third class of models is similar to the second, but it replaces the sharp threshold of equation (4) with the continuous transition found in numerical simulations by Gnedin (2000), Hoeft et al. (2006), and Okamoto et al. (2008). The numerical results in these papers can be described fairly well by a formula similar to that in Gnedin (2000), with the fraction of baryons that cool in low mass halos suppressed by a factor $[1 + 0.26(V_{\rm crit}/V_{\rm circ})^3]^{-3}$; well after the reionization redshift, the critical velocity is found to be approximately independent of redshift. Gnedin (2000) found $V_{\rm crit} \sim 40\,{\rm km\,s^{-1}}$, but these results were artificially affected by numerical resolution (N. Gnedin, private communication). Hoeft et al. (2006) and Okamoto et al. (2008) find $V_{\rm crit} \sim 25 - 30\,{\rm km\,s^{-1}}$. Including the pre-reionization contribution to M_*, this model (Model 3A) becomes

$$M_* = \frac{f_* \times (M_{\rm sat} - M_{\rm rei})}{(1 + 0.26\,(V_{\rm crit}/V_{\rm circ}(z_{\rm sat}))^3)^3} + f_* \times M_{\rm rei}\ . \quad (5)$$

The assumption that all halos can form stars before $z_{\rm rei}$ may not be justified because in halos with virial temperature $T_{\rm vir} \lesssim 10^4\,{\rm K}$ ($V_{\rm circ} \lesssim 10\,{\rm km\,s^{-1}}$) the gas does not get hot enough to cool by atomic processes, and simulations that include molecular cooling suggest that gas cooling and star formation is very inefficient in such halos (Haiman et al. 1997; Barkana & Loeb 1999; Machacek et al. 2001; Wise & Abel 2007; O'Shea & Norman 2008; Bovill & Ricotti 2008). We will therefore consider variant models (Model 3B) that eliminate stellar mass in pre-reionization halos below a critical threshold $V_{\rm crit,r} \sim 10\,{\rm km\,s^{-1}}$.[8] In Model 3B, halos with $V_{\rm circ}(z_{\rm rei}) < V_{\rm crit,r}$ have stellar mass

$$M_* = \frac{f_* \times M_{\rm sat}}{(1 + 0.26\,(V_{\rm crit}/V_{\rm circ}(z_{\rm sat}))^3)^3}\ , \quad (6)$$

while halos with $V_{\rm circ}(z_{\rm rei}) > V_{\rm crit,r}$ have mass given by equation (5).

To determine very roughly the plausible range of values for the stellar mass fraction f_*, we can refer to the results of Strigari et al. (2007), who derived $M(< r_{\rm tidal})/L) = 30 - 800 M_\odot/L_\odot$ for the classical dwarfs, and Simon & Geha (2007), who measured velocity dispersions for SDSS dwarfs and inferred total mass-to-light ratios of $140 - 1800 M_\odot/L_\odot$. For a stellar mass-to-light ratio $M_*/L_V = 1 M_\odot/L_\odot$, we infer plausible values of $f_* \sim 10^{-4} - 10^{-2}$, though these are very uncertain because all the dynamical mass-to-light ratio determinations suffer from the fact that the stars in luminous bodies of the dSphs probe only the inner parts of the dark matter potential wells. Another line of argument comes from matching the mean space density of dark matter halos to that of observed *field* dwarfs: Tinker & Conroy (2008) find $f_* \approx 10^{-3.6}$ at absolute magnitude $M_r \approx -10$. In the rest of the paper, we will frequently refer to the stellar mass fraction normalized by the universal baryon fraction:

$$F_* \equiv \frac{f_*}{\Omega_b/\Omega_m} = 6.25 f_*. \quad (7)$$

Note that f_* and F_* refer to stellar fractions in halos where the efficiency is *not* suppressed, i.e., $V_{\rm circ}(z_{\rm sat}) > V_{\rm crit}$. We will frequently refer to the quantity $(M_*/M_{\rm sat}) \times (\Omega_m/\Omega_b)$ as the "star formation efficiency," by which we mean the efficiency with which the halo converted the baryons available to it at $z_{\rm sat}$ (for a universal baryon fraction) into stars observable at $z = 0$.

TABLE 1
List of models used

Model Name	Present-Epoch Stellar Mass
1A	$M_* = f_* \times M_{\rm sat}$
1B	$M_* = f_* \times \mathtt{min}((M_{\rm sat}/M_0)^\alpha, 1) \times M_{\rm sat}$
2	$M_* = \begin{cases} f_* \times M_{\rm sat} & \text{if } V_{\rm circ}(z_{\rm sat}) > V_{\rm crit} \\ f_* \times M_{\rm rei} & \text{if } V_{\rm circ}(z_{\rm sat}) < V_{\rm crit} \end{cases}$
3A	$M_* = \frac{f_* \times (M_{\rm sat} - M_{\rm rei})}{(1+0.26\,(V_{\rm crit}/V_{\rm circ})^3)^3} + f_* \times M_{\rm rei}$
3B	same as 3A for halos with $V_{\rm circ}(z_{\rm rei}) > V_{\rm crit,r}$, for halos with $V_{\rm circ}(z_{\rm rei}) < V_{\rm crit,r}$ $M_* = \frac{f_* \times M_{\rm sat}}{(1+0.26\,(V_{\rm crit}/V_{\rm circ})^3)^3}$

3.2. *Detectability and observable properties for the simulated satellites*

Color-magnitude diagrams for the faint dwarf spheroidal galaxies in the Milky Way halo show that the stellar populations are predominantly 'old' (older than several Gyrs) and metal poor ([Fe/H]$\lesssim -1$). To convert stellar masses to luminosities, we assume that all of our model dwarfs have a stellar mass-to-light ratio $M_*/L_V \approx 1 M_\odot/L_\odot$ appropriate to an old, metal poor population (Bruzual & Charlot 2003; Martin et al. 2008). The light of the lowest luminosity dwarfs can be dominated by a handful of bright stars and thus subject to stochastic variations. We ignore this complication; our "luminosities" are simply scaled stellar masses: $L_{\rm V}/L_\odot = M_*/M_\odot$. This seems appropriate, since the luminosities of the dwarfs galaxies are usually measured either by integrating over the luminosity function of old stellar population matched to the observed luminosity function of stars in dwarfs(Belokurov et al. 2006) or by averaging over possible stochastic variations of galaxy luminosity(Martin et al. 2008).

The detectability of a faint stellar MW satellite galaxy in an SDSS-like search depends on its luminosity and its distance from the Sun, as quantified by Koposov et al. (2008) (see also Walsh et al. 2008). On the basis of these results (Figure 12 of Koposov et al. 2008) we model the detectability of each simulated satellite as a binary deci-

[8] We will refer to these as models with "pre-reionization suppression," but this simply means that halos with $V_{\rm circ}(z_{\rm rei})$ below a critical threshold form stars with very low efficiency (too low to produce observable satellites), most likely because of inefficient cooling rather than active feedback.

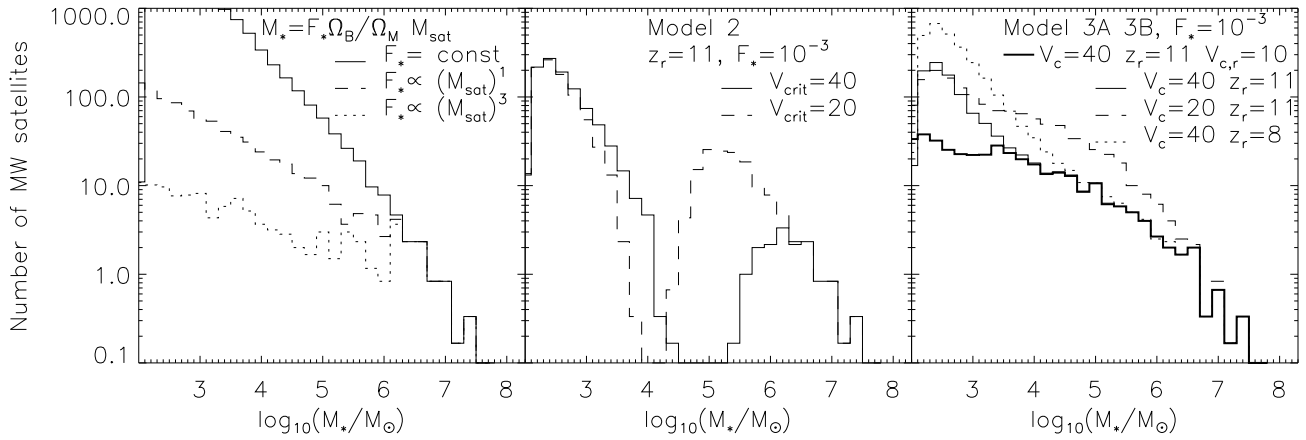

FIG. 3.— Predicted stellar mass functions of all satellites within the MW's virial radius (280 kpc), for a variety of models. *Left panel*: The solid, dotted, and dashed lines represent, respectively, Model 1A with $F_* = 10^{-3}$ and Model 1B with $(F_*, M_0, \alpha) = (10^{-3}, 10^{10}\,M_\odot, 1)$ and $(10^{-3}, 10^{10}\,M_\odot, 2)$. *Middle panel*: The two curves show predictions of Model 2, with $F_* = 10^{-3}$, $z_{\rm rei} = 11$, and $V_{\rm crit} = 40\,{\rm km\ s^{-1}}$ (*solid*), and $V_{\rm crit} = 20\,{\rm km\ s^{-1}}$ (*dashed*). *Right panel*: Thin solid, dashed, and dotted lines represent Model 3A with $(F_*, V_{\rm crit}, z_{\rm rei}) = (10^{-3}, 40\,{\rm km\ s^{-1}}, 11)$, $(10^{-3}, 30\,{\rm km\ s^{-1}}, 11)$, and $(10^{-3}, 40\,{\rm km\ s^{-1}}, 8)$, respectively. The thick solid curve shows model 3B with $F_* = 10^{-3}$, $V_{\rm crit} = 40\,{\rm km\ s^{-1}}$, $z_{\rm rei} = 11$, and $V_{\rm crit,r} = 10\,{\rm km\ s^{-1}}$. All curves reflect the average of six realizations of MW halos. These are the predicted *complete* satellite (stellar) mass functions, with no radial or sky coverage selection effects.

sion using the criterion

$$\log_{10}(D_\odot/1\,{\rm kpc}) < 1.1 - 0.228 M_V \qquad (8)$$

Our simulations provide the current Galactocentric distance and orbital apocenter and pericenter for each sub-halo, but not the orientation of the orbit. We therefore assign the heliocentric distance of the satellites

$$D_\odot = \sqrt{8.5^2 + D_{GC}^2 - 2 \times 8.5 \times D_{GC} \cos(\phi)}\ , \qquad (9)$$

where D_{GC} is the Galactocentric distance (in kpc) from the simulations and $\cos(\phi)$ is a random variable uniformly distributed between -1 and 1 (ϕ is the angle between radial vectors from the GC to the Sun and to the sub-halo). This method assumes that the satellite orbits are isotropically distributed across the sky (see Tollerud et al. 2008, for discussion of the validity of this approximation). As expected from Koposov et al. (2008), accounting for the detectability of satellites causes the 'observable' population to differ strongly from the 'simulated' one; only the brightest satellites are observable throughout the virial volume.

Not surprisingly, the Koposov et al. (2008) analysis also reveals a surface brightness threshold for dwarf detection, which is approximately 30 mag arcsec^{-2} with little dependence on distance. We assume that any model dwarf that passes the luminosity threshold also passes the surface brightness threshold. Many recent SDSS satellite discoveries do lie near that survey's surface brightness limit; this assumption can therefore only be tested with the next generation of sky surveys. We discuss implications of this assumption in §5.

With a model that assigns stellar luminosities to each satellite halo, we can predict the expected stellar velocity dispersions for comparison with those measured for MW satellites by Walker et al. (2007), Simon & Geha (2007), and Martin et al. (2007). This can be done straightforwardly if we assume that the stars are test particles — an assumption supported by the observed $(M/L)_{\rm dyn}(< R_{\rm eff}) \gg (M/L)_*(< R_{\rm eff})$ — orbiting in an NFW potential with an isotropic velocity dispersion. Then we can use the Jeans equation (Jeans 1919) to derive the velocity dispersion profile of stars:

$$\frac{d(\nu(r)\,\sigma^2(r))}{d\,r} + \nu(r)\,\frac{G\,M(r)}{r^2} = 0, \qquad (10)$$

where ν is the density distribution of stars (see Strigari et al. 2007 for more detailed treatment). Here we assume that the density of stars follows a Plummer profile $\nu \propto [1 + (r/r_p)^2]^{-2}$ (Plummer 1911), which seems to fit observed density profiles reasonably well (Wilkinson et al. 2002; Belokurov et al. 2007). The mass profile $M(r)$ used here is computed based on the virial radii and concentrations at the redshift $z_{\rm sat}$ of sub-halo accretion. While the outer parts of the sub-halos are tidally stripped, Peñarrubia et al. (2008) show that the stars and the inner part of the dark matter sub-halo are stripped only at a very late stage, when the sub-halo is close to complete disruption. They also show that the velocity dispersion in sub-halos is a function of the total dark matter mass remaining bound inside the luminous body and therefore remains nearly constant until this late stage.

After numerically solving the Jeans Equation, we compute the expected light-weighted velocity dispersion within the optical radius as

$$\sigma_* = \frac{\int \nu(r)\sigma(r)\,dx\,dy\,dz}{\int \nu(r)\,dx\,dy\,dz}, \qquad (11)$$

where the integration is done over a cylinder within a radius, $R = \sqrt{x^2 + y^2}$ equal to the Plummer radius of the galaxy; the integral extends over $\pm\infty$ in z. The stellar velocity dispersion depends on the radial extent of the stellar tracers, which cannot be predicted within our simple modeling context (see also Benson et al. 2002). We therefore use the *observed* properties of the faint Milky Way satellites to choose stellar radii, based on Martin et al. (2008). Specifically, we adopt Plummer radii $r_p = 150$ pc for $M_V < -5$, and for fainter dwarfs

we adopt a linear relation between log r_p and M_V with r_p rising from 20 pc at $M_V = 0$ to 150 pc at $M_V = -5$.

The additional important component of the detectability is the tidal disruption of the satellite galaxies. Although our semi-analytic model of dark matter sub-halo evolution properly accounts for the tidal disruption of sub-halos, it does not allow for the possibility that stars have been dispersed in a tidal stream while a small core of the sub-halo survives. Here we simply classify a sub-halo as unobservable if its current tidal radius is less than the expected Plummer radius of the stellar body, which would imply substantial tidal disruption of the stellar component. We also presume that a satellite is unobservable if its host sub-halo has lost more than 99% of its original mass to tidal stripping.

4. RESULTS

4.1. *Stellar mass function of the full satellite populations*

Figure 3 shows the predicted distribution of the *stellar* masses of satellites within $R_{\rm virial} = 280$ kpc, assuming 4π sky coverage and complete satellite detectability. In the left panel, the solid curve shows Model 1A with a constant $F_* = 10^{-3}$, making the stellar mass function a scaled version of the dark matter sub-halo mass function. Introducing mass-dependent suppression, Model 1B with $\alpha = 1$ (dashed) and $\alpha = 2$ (dotted) lowers the low mass end of the stellar mass function as expected. Since this model also adopts $F_* = 10^{-3} =$ const. above $M_{\rm sat} = M_0 = 10^{10} M_\odot$, the high mass end of the mass function is unchanged.

The middle panel of Figure 3 shows Model 2, with post-reionization suppression of star formation in halos below a sharp circular velocity threshold, either $V_{\rm crit} = 40\,{\rm km\ s^{-1}}$ (solid) or $V_{\rm crit} = 20\,{\rm km\ s^{-1}}$ (dashed), where we have adopted $F_* = 10^{-3}$ and a reionization redshift $z_{\rm rei} = 11$. The resulting stellar mass functions for the satellite galaxies are strongly bimodal, with the low mass portion corresponding to dwarfs in which all stars formed before reionization and the high mass portion corresponding to halos that exceeded the critical velocity threshold before becoming satellites, $V_{\rm circ}(z_{\rm sat}) > V_{\rm crit}$. The low mass portion is just a scaled version of the sub-halo mass function at $z = z_{\rm rei}$. Above $M_* \approx 10^{6.5} M_\odot$ the host halos are all massive enough to have star formation after $z_{\rm rei}$, and the mass function is the same as that of Model 1. If the velocity threshold is lowered to $V_{\rm crit} = 20\,{\rm km\ s^{-1}}$, the high mass peak in the distribution of satellite stellar masses extends to lower values before photo-ionization suppression cuts it off.

The bimodal appearance of the middle panel of Figure 3 is a direct consequence of the sharp $V_{\rm circ}$ threshold for photo-ionization suppression. The right hand panel shows predictions for several variants of Model 3A and 3B, with the Gnedin (2000) formula (Eq. 5) used to describe photo-ionization suppression. With this smooth suppression, the "pre-reionization" and "post-reionization" portions of the mass function join to make a smooth overall mass function. The low mass end of the mass function is now a mix of satellites that formed their stars before reionization and satellites with $V_{\rm circ}(z_{\rm sat}) < V_{\rm crit}$ whose post-reionization star formation was strongly suppressed but not completely eliminated. Lowering the assumed reionization redshift from $z_{\rm rei} = 11$ to $z_{\rm rei} = 8$ boosts the stellar mass function below $M_* = 10^4 M_\odot$. Conversely, if we eliminate pre-reionization SF in dwarfs with $V_{\rm circ}(z_{\rm rei}) < V_{\rm crit,r} = 10\,{\rm km\ s^{-1}}$ (thick solid line, Model 3B), the number of satellites with $M_* \leq 10^3 M_\odot$ drops by a large factor, while at higher masses the stellar mass function is unaffected. The difference between the thin and thick solid lines is the contribution of satellites that formed stars primarily before reionization in halos with $V_{\rm circ}(z_{\rm rei}) < 10\,{\rm km\ s^{-1}}$, for $z_{\rm rei} = 11$ and $V_{\rm crit} = 40\,{\rm km\ s^{-1}}$.

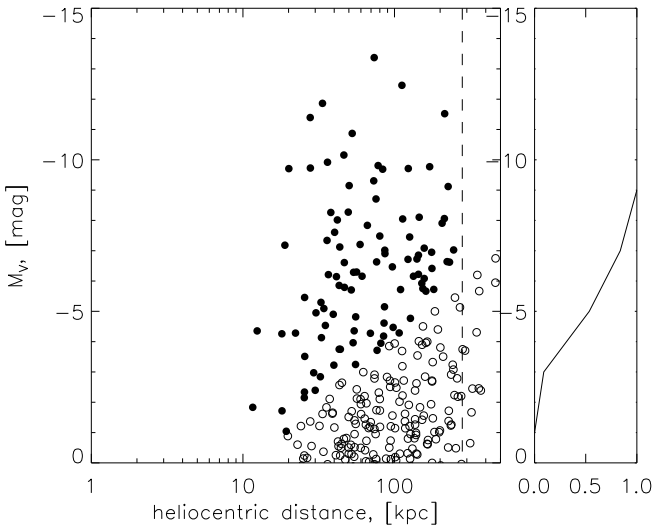

FIG. 4.— Detectability of the satellite galaxies predicted by our fiducial model (Model 3B), as a function of their heliocentric distance and stellar luminosity. Filled circles denote galaxies that can be detected with SDSS-like all-sky surveys, and empty circles denote those that cannot. The dashed line marks the approximate virial radius of the MW's dark matter halo; we will compare all model predictions to the observed MW satellite population only within this radius. The galaxies shown were taken from one Monte-Carlo realization of Model 3B with $(V_{\rm crit}, F_*, z_{\rm rei}, V_{\rm crit,r}) = (35\,{\rm km\ s^{-1}}, 10^{-3}, 11, 10\,{\rm km\ s^{-1}})$. The right panel shows the fraction of detectable galaxies as a function of luminosity.

4.2. *Distribution of observed dwarf satellite luminosities, $N(M_V)$*

Figure 4 illustrates the impact of selection effects on the observable satellite population. For one realization of Model 3B (with parameters that yield a good match to observations), filled circles show satellites that would be detectable in an all-sky, SDSS-like survey (Koposov et al. 2008), and open circles show un-detectable satellites. The low end of the luminosity distribution, with $M_V \gtrsim -5$, is strongly affected by the radial selection bias.

For direct comparison with observations, we therefore select only those model satellites whose combination of luminosity and distance would make them detectable. At the bright end, $M_V < -11$, we assume that existing photographic surveys are complete to $D_\odot = 280$ kpc, and we thus compare the total number of dwarfs across the whole sky to the total population of satellites within the virial radius in the simulation. For $M_V \geq -11$, we randomly select 1/5 of the model galaxies to mimic the 20% sky coverage of SDSS DR5, and we count only those satellites that would be detectable according to the criteria of

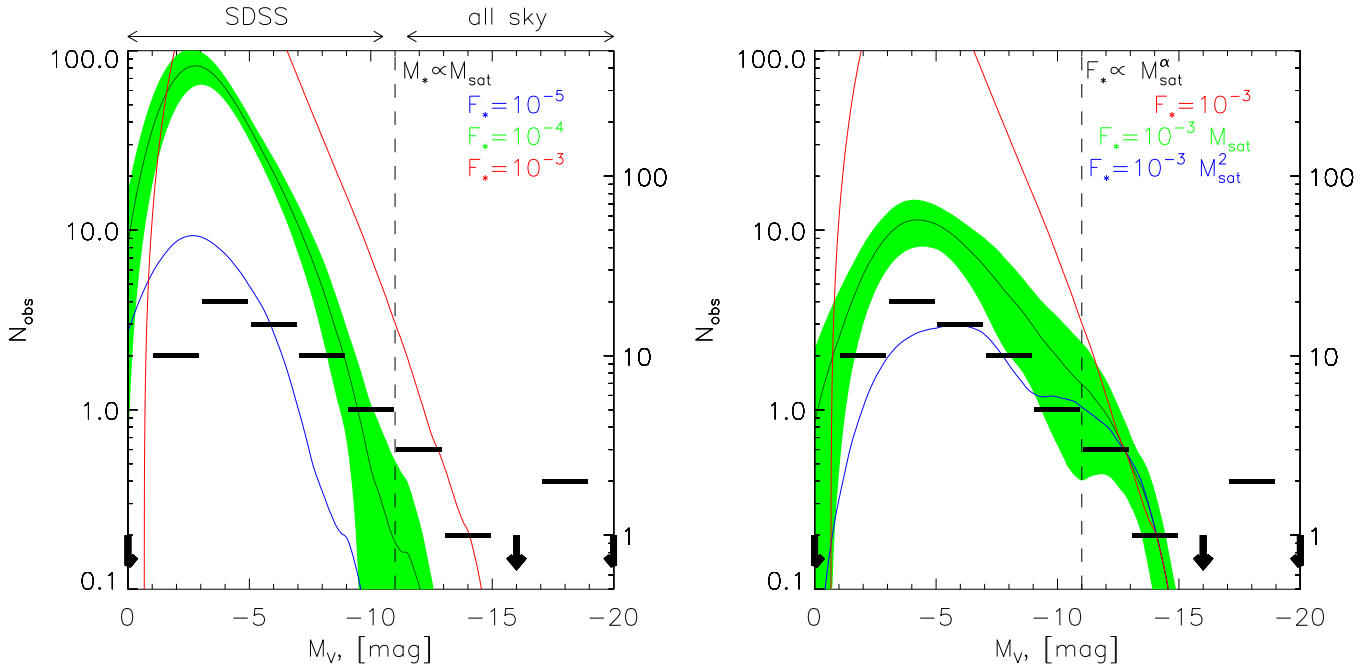

FIG. 5.— Model predictions for the observed satellite population, $N_{\rm obs}(M_V)$, including radial selection effects for the SDSS dwarfs. Horizontal bars show the number of currently known satellites (Table 2) in 2-magnitude bins; empty bins are plotted with an arrow. The SDSS and classical dwarfs are separated by the vertical line at $M_V = -11$; note that the y-axes for these two populations differ by a factor of five so that the model predictions (which incorporate a factor of 1/5 below $M_V = -11$ to account for SDSS sky coverage) are continuous across the boundary. *Left Panel:* Predictions of Model 1A, with $M_* \propto M_{\rm sat}$, for three values of F_*. For $F_* = 10^{-4}$, the green band shows the bin-by-bin $\pm 1\sigma$ range of the predictions from multiple realizations; the logarithmic width of this band is similar for other models. Model curves have been slightly smoothed with a polynomial filter. *Right Panel:* Comparison of Model 1A (red curve) to Model 1B, where the stellar mass fraction in halos with $M_{\rm sat} < 10^{10} M_\odot$ is is $F_* \propto M_{\rm sat}^\alpha$, with $\alpha = 1$ (green band) or $\alpha = 2$ (blue curve).

Koposov et al. (2008). We focus our data-model comparison on $N_{\rm obs}(M_V)$, the luminosity distribution of known MW satellites. We look at additional tests against stellar velocity dispersions, central masses, and the heliocentric radial distribution in § 4.3.

The luminosities, distances, and velocity dispersions of the observed Milky Way satellites that we use in all subsequent model - data comparisons were taken from various authors (Mateo 1998; Metz & Kroupa 2007; Martin et al. 2008) and are compiled in Table 2. The sample of SDSS satellites used here consists of those systems above the 50% completeness limits of Koposov et al. (2008). We do not include two systems, BooII and LeoV (Walsh et al. 2007; Belokurov et al. 2008), which do not formally satisfy the very conservative selection limits from Koposov et al. (2008) These limits were chosen to avoid the issue of significant 'false positive' detections, at the expense of leaving out 2 objects that deeper follow-up found to be 'real'. For the analysis presented here it is most important that the *same* selection criteria are applied to the mock satellite observations and the SDSS data. As our analysis subsequently shows, such a small difference in sample size is smaller than the model halo to halo variation of number of galaxies. Therefore the inclusion of omission of these two objects does not affect our results significantly.

Anyway, as we will see later, the halo to halo variation of number of galaxies in our models is noticeable, so we believe that the fact that we do not include two galaxies should not affect our results significantly.

The left panel of Figure 5 compares our simplest model ($M_* \propto M_{\rm sat}$, Model 1A) to the observed satellite counts, now including the satellite galaxy selection effects in the model. We randomly sample each of the six Monte Carlo halo simulations five times (choosing 1/5 of the faint satellites but always keeping the full set for $M_V < -11$), compute the mean model prediction as the mean of these 30 samplings, and compute the rms dispersion among these 30 in each absolute magnitude bin. Despite the selection bias against low luminosity satellites, this model fails drastically for any choice of F_*, predicting a much steeper luminosity function than observed. For example, the model with $F_* = 10^{-4}$ matches the observed counts near $M_V = -9$ but predicts far too many satellites fainter than $M_V = -6$. Selection effects and newly discovered satellites have not altered this basic discrepancy, first emphasized by Klypin et al. (1999) and Moore et al. (1999). The green band shows the 1σ dispersion in predicted counts, and it is clear that statistical fluctuations will not resolve the discrepancy either.

In the right panel we apply our purely empirical modification, $M_*/M_{\rm sat} \propto M^\alpha$ below a halo mass $M_{\rm sat} = M_0 = 10^{10} M_\odot$ (Model 1B). With $F_* = 10^{-3}$ and $\alpha = 2$, this model achieves reasonable agreement with the the observed $N_{\rm obs}(M_V)$ over the full range $0 \geq M_V \geq -15$. The agreement can be further improved by adjusting F_* and M_0, so it appears that this level of mass-dependent suppression is approximately what is needed to explain the observed shape of $N_{\rm obs}(M_V)$. Linear suppression ($\alpha = 1$, green band) is not sufficient, predicting an excess of faint dwarfs when normalized to the bright dwarfs. All of our models fail to match the brightest bin (comprised of the SMC and LMC); we defer discussion of this discrepancy to the end of this Section.

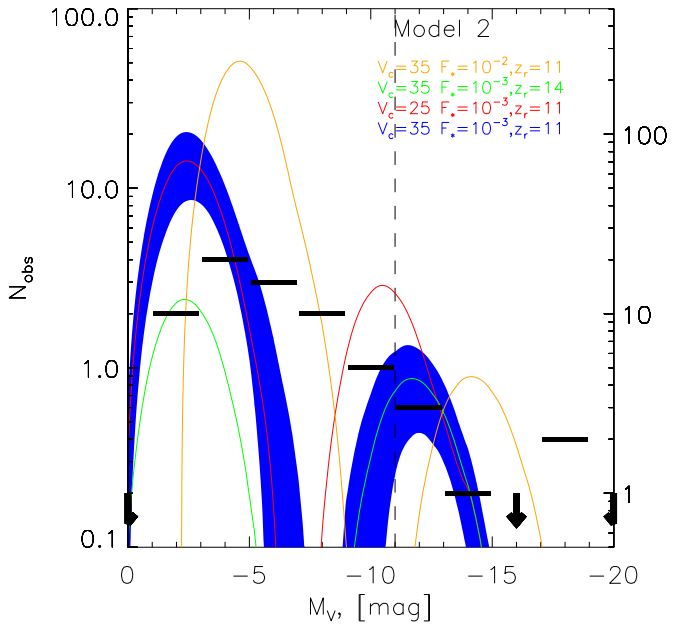

FIG. 6.— Predictions for Model 2, in which post-reionization star formation is sharply suppressed below a critical velocity $V_{\rm crit}$, in the same format as Figure 5. Blue, red, green, and orange curves/bands show the parameter combinations $(F_*, V_{\rm crit}, z_{\rm rei}) = (10^{-3}, 35\,{\rm km\ s^{-1}}, 11)$, $(10^{-3}, 25\,{\rm km\ s^{-1}}, 11)$, $(10^{-3}, 35\,{\rm km\ s^{-1}}, 14)$, and $(10^{-2}, 35\,{\rm km\ s^{-1}}, 11)$, respectively. This class of models predicts a bimodal distribution of satellite luminosities, with the faint portion ($M_V > -8$) coming entirely from pre-reionization star formation. The predicted $N(M_{\rm V})$ differs grossly from the observations.

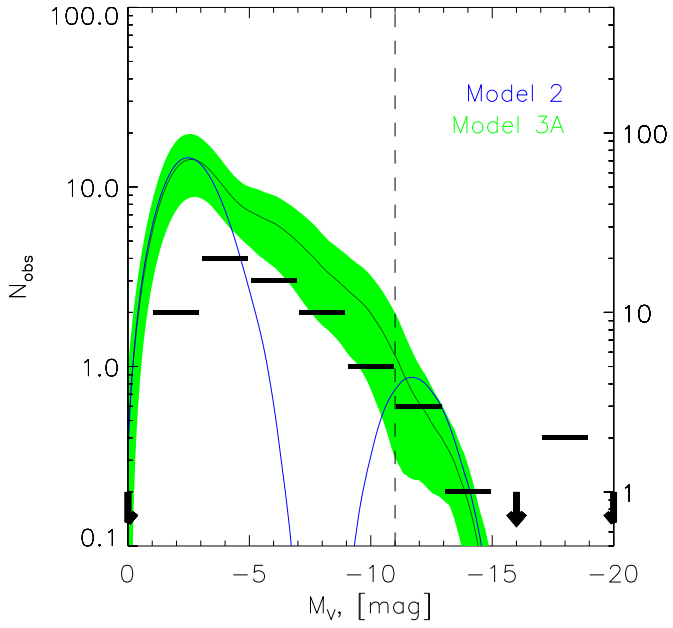

FIG. 7.— Comparison of Model 2 and Model 3A, both with parameters $F_* = 10^{-3}$, $V_{\rm crit} = 35\,{\rm km\ s^{-1}}$, and $z_{\rm rei}$=11, in the same format as Figure 5. Switching to the continuous prescription for photo-ionization suppression fills in the gap between the two peaks of Model 2, while leaving the predictions at the highest and lowest luminosities unchanged.

Figure 6 shows the expected $N_{\rm obs}(M_V)$ distributions for Model 2, which has a sharp $V_{\rm crit}$ threshold for the suppression of SF after reionization in small halos. As in Figure 3, the predicted $N_{\rm obs}(M_V)$ is bimodal, with a bright peak corresponding to halos that exceeded $V_{\rm crit}$ before $z_{\rm sat}$ and a faint peak corresponding to stars formed before reionization. Raising the stellar fraction F_* with other parameters fixed (orange vs. blue) shifts both peaks horizontally to higher M_V; the faint peak also increases in height because the brighter (though still faint) satellites can be seen over a larger fraction of the MW virial volume. Lowering $V_{\rm crit}$ with other parameters fixed (red vs. blue) has no impact on the faint peak, but the bright peak extends to fainter magnitudes and grows in height because lower mass halos can now be populated with stars after reionization. Raising $z_{\rm rei}$ (green vs. blue) with other parameters fixed has no impact on the bright peak, but it shifts the faint peak downwards in amplitude and slightly downwards in location because halos have accreted less mass by this higher redshift. While photo-ionization suppression reduces the discrepancy with the number of faint satellites seen in Model 1A, these sharp threshold models predict a gap between the faint and bright satellites that is clearly at odds with the data.

Figure 7 compares the Model 2 predictions with those of Model 3A, which uses the Gnedin (2000) formula to incorporate a smoothly increasing suppression of the stellar mass fraction in halos with $V_{\rm circ}(z_{\rm sat}) \lesssim V_{\rm crit}$. In both cases we use parameters $F_* = 10^{-3}$, $V_{\rm crit} = 35\,{\rm km\ s^{-1}}$, $z_{\rm rei} = 11$. Model 3A is more physically realistic than Model 2, with a mass-dependent suppression that is calibrated on numerical simulations (and is approximately consistent with three independent numerical studies). Galaxies formed in halos with $V_{\rm circ}(z_{\rm sat}) \lesssim V_{\rm crit}$ now fill the gap that was present in Model 2, producing a luminosity distribution that rises continuously from $M_V = -14$ down to $M_V = -2$, before radial selection effects finally cut it off. With these parameter choices, pre-reionization dwarfs dominate the counts (and exceed the observations) for $M_V \leq -4$, but suppressed post-reionization dwarfs dominate the counts at all brighter magnitudes.

Since Model 3 is both more physically realistic and more empirically successful than Models 1 and 2, we focus on it for the remainder of the paper, including Model 3B in which pre-reionization star formation is suppressed below a circular velocity threshold. Figure 8 systematically explores the impact of parameter variations in Models 3A and 3B. In the first three panels, the green band shows the Model 3A predictions for a fiducial set of parameter choices, $F_* = 10^{-3}$, $V_{\rm crit} = 35\,{\rm km\ s^{-1}}$, and $z_{\rm rei} = 11$. Changing F_* (top left) shifts the predicted distribution horizontally to higher or lower luminosities, with some change in shape at the faint end because of the luminosity dependence of radial selection effects. Changing $V_{\rm crit}$ alters the predicted counts at intermediate luminosities, $-4 > M_V > -11$, while having little effect at the faint end (where pre-reionization dwarfs dominate) or at the bright end (where most galaxies exceed the highest threshold considered here). Changing $z_{\rm rei}$ alters the height of the pre-reionization peak at faint luminosities but has minimal impact for $M_V < -7$.

With our fiducial parameter choices, Model 3A sub-

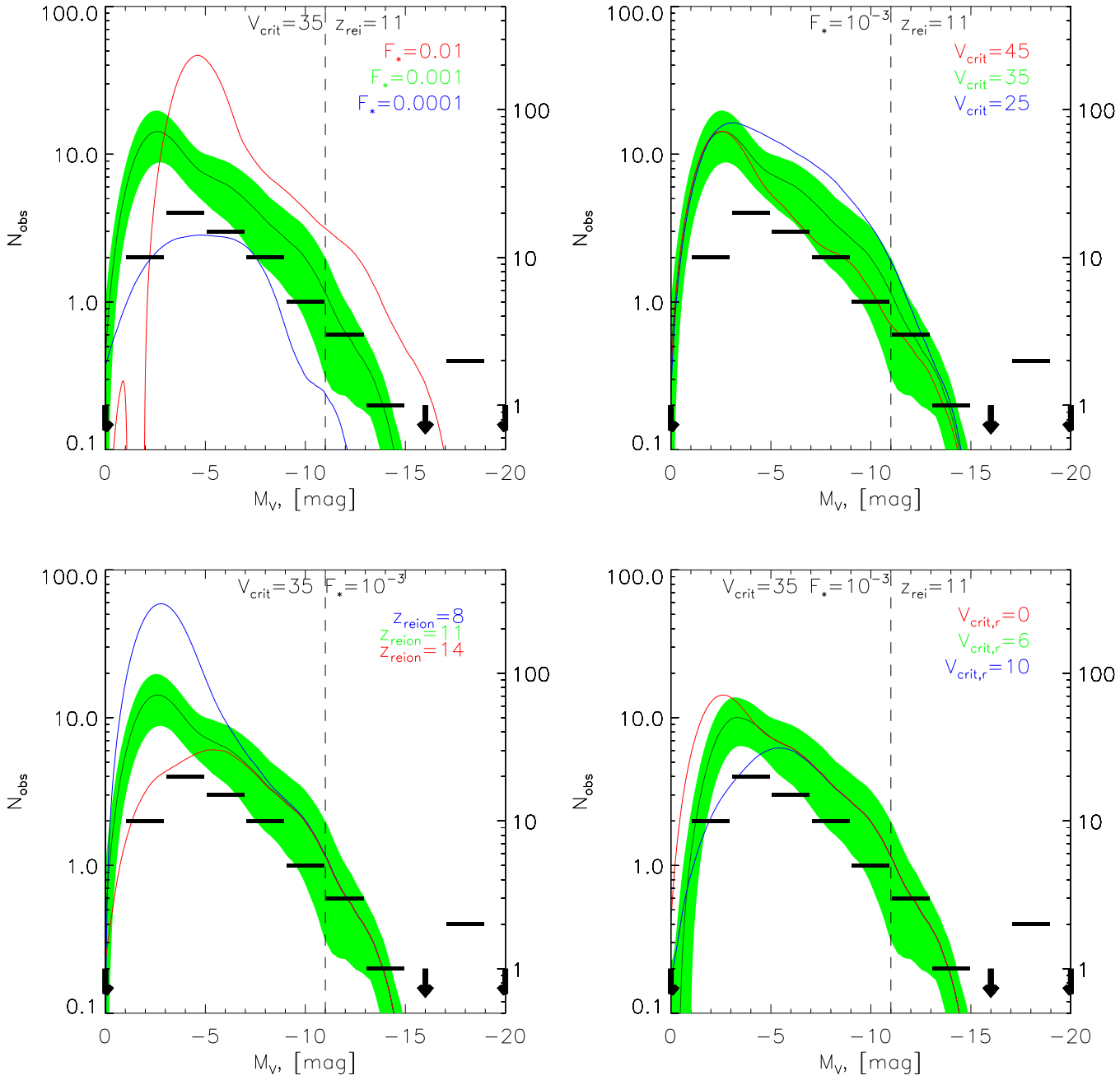

FIG. 8.— Predicted $N_{\rm obs}(M_V)$ for Models 3A and 3B with a variety of parameter choices, in the same format as Figure 5. In the first three panels, green bands show Model 3A predictions for a reference parameter set $F_* = 10^{-3}$, $V_{\rm crit} = 35\,{\rm km\ s^{-1}}$, $z_{\rm rei} = 11$. Red and blue curves show the impact of changing the stellar mass fraction to $F_* = 10^{-2}$ or 10^{-4} (top left), the critical velocity threshold to $V_{\rm crit} = 45\,{\rm km\ s^{-1}}$ or $25\,{\rm km\ s^{-1}}$ (top right), or the reionization redshift to $z_{\rm rei} = 8$ or 14 (lower left). The lower right panel compares the prediction of this reference model (now shown by the red curve) to predictions of Model 3B with a pre-reionization critical threshold $V_{\rm crit,r} = 6\,{\rm km\ s^{-1}}$ (green band) or $10\,{\rm km\ s^{-1}}$ (blue curve).

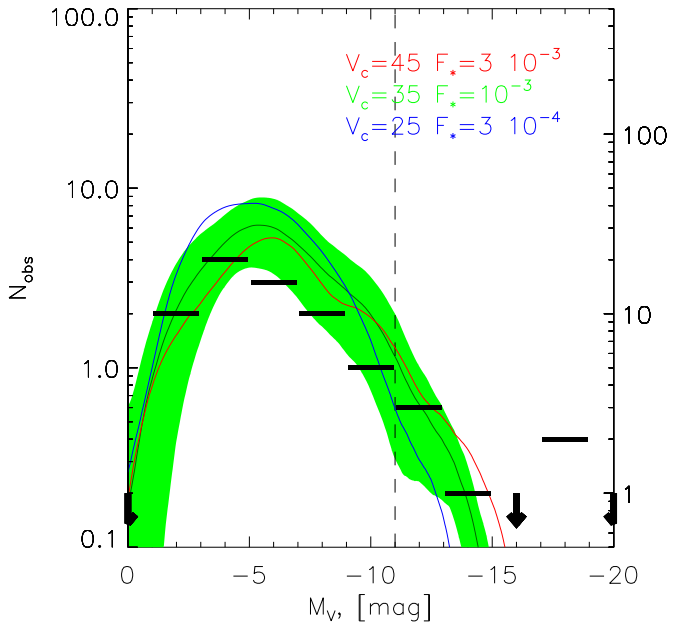

FIG. 9.— Degeneracy between F_* and $V_{\rm crit}$ for Model 3B, in the format of Figure 5. Blue, green, and red curves/bands show the parameter combinations $(F_*, V_{\rm crit}) = (3\times10^{-4}, 25\,{\rm km\ s^{-1}})$, $(10^{-3}, 35\,{\rm km\ s^{-1}})$, and $(3\times10^{-3}, 45\,{\rm km\ s^{-1}})$, which all yield similar levels of agreement with the observations. We adopt $z_{\rm rei} = 11$ and $V_{\rm crit,r} = 10\,{\rm km\ s^{-1}}$ in all cases.

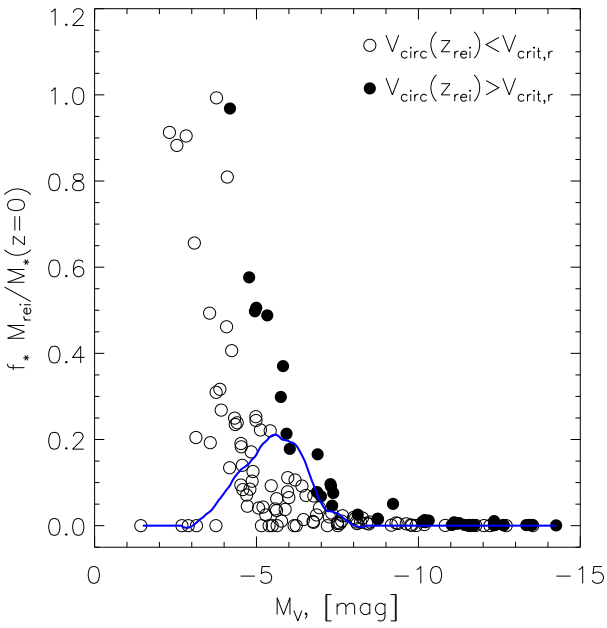

FIG. 10.— Fraction of pre-reionization stars in observable satellites of different luminosities, as predicted by the fiducial Model 3B. Filled circles show $f_* M(z_{\rm rei})/M_*(z=0)$, the fraction of the stellar mass that formed by $z_{\rm rei}$, for systems that exceeded the pre-reionization threshold, $V_{\rm circ}(z_{\rm rei}) > V_{\rm crit,r} = 10\,{\rm km\ s^{-1}}$. Open circles show $f_* M(z_{\rm rei})/M_*(z=0)$ for systems with $V_{\rm circ}(z_{\rm rei}) < V_{\rm crit,r}$, but in the context of Model 3B these systems do not form any stars before reionization. The curve shows the fraction of satellites that formed more than 10% of their stars before the epoch of reionization, in bins of luminosity.

stantially overpredicts the number of satellites with $M_V \approx -3$. Raising the reionization redshift to $z_{\rm rei} = 14$ erases this discrepancy, but this value of $z_{\rm rei}$ seems implausible given the strong and rapidly evolving opacity of the intergalactic medium at $z \approx 6$ seen in quasar spectra (Fan et al. 2006), and it is only marginally consistent with the WMAP5 results. In the lower right panel, we return to $z_{\rm rei} = 11$ but suppress pre-reionization star formation in halos with $V_{\rm circ}(z_{\rm rei}) < 6\,{\rm km\ s^{-1}}$ (green) or $10\,{\rm km\ s^{-1}}$ (blue), motivated by the inefficient gas cooling expected below the threshold for atomic line excitation (Model 3B). The $V_{\rm crit,r} = 10\,{\rm km\ s^{-1}}$ model yields acceptable agreement with the observed number counts over the full range $0 \geq M_V \geq -15$. The $V_{\rm crit,r} = 6\,{\rm km\ s^{-1}}$ model still yields an excess of faint satellites; results for $V_{\rm crit,r} = 8\,{\rm km\ s^{-1}}$ (not shown) are nearly identical to those for $10\,{\rm km\ s^{-1}}$, indicating that an $8\,{\rm km\ s^{-1}}$ threshold is already sufficient to essentially eliminate the contribution of pre-reionization dwarfs. This pre-reionization suppression appears to be critical to explaining the number of dwarfs observed by the SDSS.

Within Model 3B, there is strong degeneracy between the values of F_* and $V_{\rm crit}$. Figure 9 shows that the parameter combinations $(F_*, V_{\rm crit}) = (3\times10^{-3}, 45\,{\rm km\ s^{-1}})$, $(10^{-3}, 35\,{\rm km\ s^{-1}})$, and $(3\times10^{-4}, 25\,{\rm km\ s^{-1}})$ all yield similar predictions and acceptable agreement with the observed number counts. The lower values of $V_{\rm crit}$ are favored by the numerical studies of Hoeft et al. (2006) and Okamoto et al. (2008). For the remainder of the paper we will adopt $(F_*, V_{\rm crit}, z_{\rm rei}, V_{\rm crit,r}) = (10^{-3}, 35\,{\rm km\ s^{-1}}, 11, 10\,{\rm km\ s^{-1}})$ as the fiducial parameter values for Model 3B.

For this fiducial model, Figure 10 illustrates in more detail the relative importance of stars formed before and after reionization. For systems with $V_{\rm circ}(z_{\rm rei}) > V_{\rm crit,r}$, filled circles show the fraction of their stars that formed before reionization. For systems with $V_{\rm circ}(z_{\rm rei}) < V_{\rm crit,r}$, open circles show the fraction of stars that *would* have formed before reionization, but because of the $V_{\rm crit,r}$ threshold these galaxies have no pre-reionization stars in this model. At every satellite luminosity, the average fraction of pre-reionization stars is small, or even zero, but albeit for different reasons at high and low luminosities. The host halos for the brighter, "classical" dwarf satellites were typically massive enough at $z_{\rm rei}$ to exceed $V_{\rm crit}$, but that initial population of stars was subsequently swamped by the much larger post-reionization population. In contrast, the halos that now host the very faintest known satellites ($M_V > -4$) did not exceed $V_{\rm crit,r}$ at $z_{\rm rei}$ and hence — in Model 3B — did not form any stars before $z_{\rm rei}$. A small fraction of the satellites with $M_V \approx -5$ have large populations of pre-reionization stars; these are sub-halos that just exceeded $V_{\rm crit,r}$ at $z_{\rm rei}$ but have low enough values of $V_{\rm circ}(z_{\rm sat})$ that their post-reionization star formation was strongly suppressed. If the pre-reionization threshold at $V_{\rm crit,r}$ were smooth rather than sharp, then some additional fainter systems might have significant fractions of pre-reionization stars. However, the general conclusion that pre-reionization star formation should be a small fractional contribution at all satellite luminosities seems fairly robust, provided this star formation is suppressed

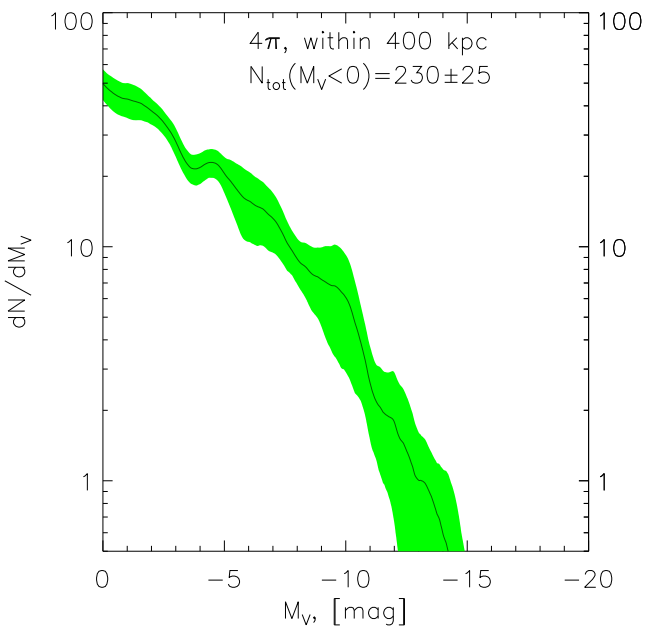

FIG. 11.— The predicted number of MW satellites per unit magnitude within 400 kpc across the whole sky averaged from 6 MC realizations, using the fiducial model parameters (Model 3B with $F_* = 10^{-3}$, $V_{\rm crit} = 35\,{\rm km\ s^{-1}}$, $V_{\rm crit,r} = 10\,{\rm km\ s^{-1}}$, and $z_{\rm rei} = 11$) and assuming no observational incompleteness. The total number of satellites with stellar luminosities brighter than $M_V = 0$ is 230 ± 25. Note that this Figure gives counts in 1-magnitude bins rather than the 2-magnitude bins used in earlier Figures.

in halos below the atomic cooling threshold, as seems to be required to match the observed luminosity distribution.

Figure 11 shows the complete stellar luminosity function of MW satellites inside 400 kpc, in the absence of any selection effects or incompleteness, again for the fiducial model. (We choose 400 kpc for ease of comparison to Tollerud et al. 2008.) In contrast to other figures, it shows the luminosity function for the whole sky (4π sr) and in terms of dN/dM_V (i.e., in bins of 1 magnitude). Absent selection effects, the luminosity function continues to rise toward faint magnitudes (as noted by Koposov et al. 2008), contrary to the almost flat luminosity distribution of observed dwarfs. The total number of satellites within 400 kpc brighter than $M_V = 0$ expected for the fiducial Model 3B is 230± 35. This value is somewhat lower than the 400 derived by Tollerud et al. (2008), but since both estimates extrapolate the number of known dwarfs by a factor of ~ 10, we do not place much weight on this difference.

None of the models shown in Figures 5–9 reproduce the brightest observed bin — i.e., they all fail to produce satellites as bright as the SMC and the LMC. Our successful models have low stellar mass fractions, $F_* \sim 10^{-3}$, even well above the photo-ionization threshold $V_{\rm crit}$. The most massive sub-halos in our Monte Carlo realizations have typical mass $M_{\rm sat} \sim 10^{11} M_\odot$ (ranging from $10^{10.5} M_\odot$ to $10^{11.4} M_\odot$), with second-ranked halos that are $0.2 - 0.4$ dex less massive. Reproducing the $\sim 10^9 M_\odot$ stellar masses of the Magellanic Clouds then requires much higher stellar mass fractions $F_* \sim 0.05$. To reproduce the full satellite population, the efficiency of gas accretion and star formation must continue to rise with halo mass above $V_{\rm crit}$, or at least it must be higher for the SMC and LMC hosts. Since the number of bright SMC and LMC-like objects in our model are determined mainly by one parameter F_*(because these objects are not suppresed by the photo-ionization), that rise of star formation efficiency can not be accomodated with our simple model without introducing additional parameters.

4.3. *Velocity dispersions, central masses, and radial distributions*

As discussed in §3.2, predicting stellar velocity dispersions requires assumptions beyond those needed to compute $N_{\rm obs}(M_V)$. In particular, we assume that the satellites' host sub-halos have NFW profiles with concentration given by the theoretically expected mean $c(M)$ relation at $z_{\rm sat}$, and that subsequent dynamical evolution (e.g., tidal stripping) does not alter the mass distribution of the inner parts of the sub-halo probed by the stars. We also take the observed stellar radii ($20 - 150$ pc, see § 3.2 for details) as input rather than predicting them from a physical model. With these assumptions, the right panel of Figure 12 shows the predicted distribution of stellar velocity dispersions for Model 3B with our fiducial parameter choices. The characteristic value and narrow spread of velocity dispersions for the newly discovered SDSS dwarfs arises quite naturally from these models, despite the large range of stellar luminosities and host sub-halo masses. The predicted distribution is more sharply peaked than the observed one, probably because we did not include scatter in the halo concentration-mass relation and did not include observational uncertainties in the dispersion measurements. The mean value of σ_* differs by $< 20\%$ between data and model, but we consider this small discrepancy is not worrisome, given the simplicity of our dynamical modeling.

The total masses of dwarf satellites are difficult to determine observationally because of the small extent of the stellar distributions relative to the expected extent of the dark matter sub-halo. However, Strigari et al. (2008) show that the total mass (principally dark matter) within a radius of 300 pc, M_{300}, can be inferred robustly from observations for nearly all of the known satellites. The top panel of Figure 13 compares the fiducial model predictions of M_{300} to the Strigari et al. (2008) measurements. The model (red diamonds) naturally reproduces the key result of Strigari et al. (2008): over an enormous range of luminosities, the satellites have a narrow range of M_{300}, tightly concentrated around $10^7 M_\odot$. The theoretical prediction is artificially tight because we have not included scatter in halo concentrations, which would produce roughly 0.15 dex (rms) of scatter in M_{300} (see Macciò et al. 2009, figure 1). The model predicts a weak trend of M_{300} with luminosity, which is not evident in the data (but is similar to that predicted by Macciò et al. 2009).

While the M_{300} range of the satellites is low, the range of *total* sub-halo masses (at $z = 0$) is more than three orders of magnitude, as shown in the middle panel of Figure 13. The trend of total mass with luminosity is much stronger than the trend for M_{300}, though there is a large scatter in mass at fixed luminosity because of tidal stripping. The near constancy of M_{300} is a consequence of the density profiles of CDM halos: NFW ha-

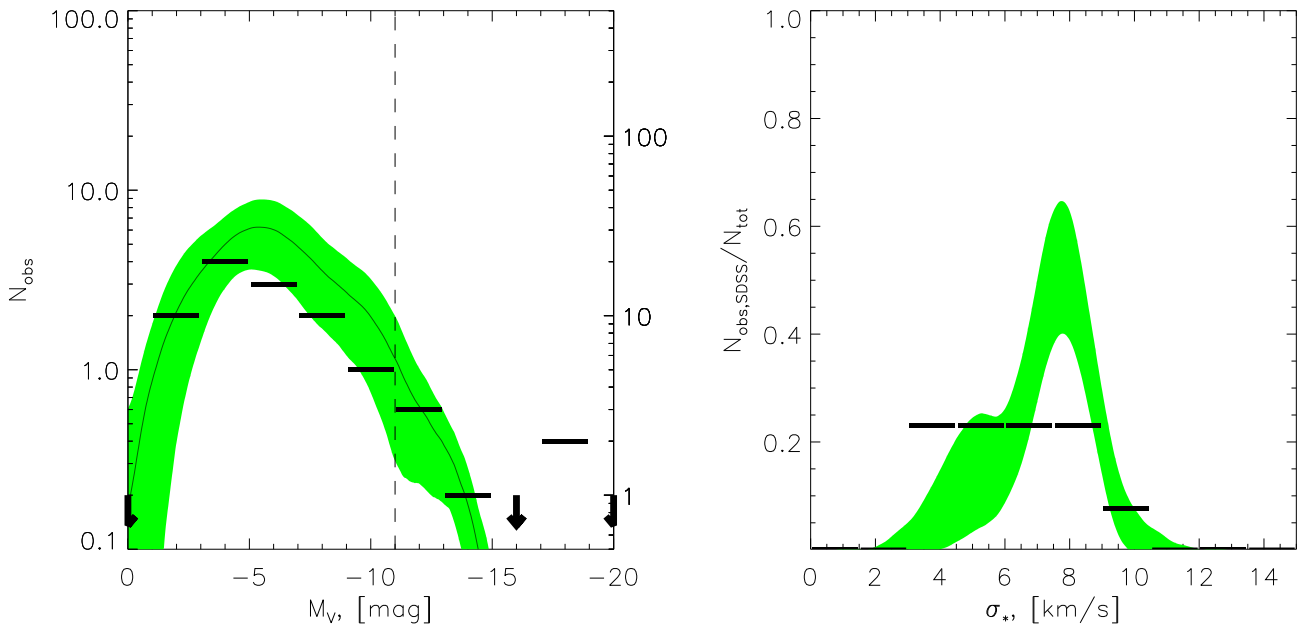

FIG. 12.— Predictions of Model 3B with the fiducial parameters $(F_*, V_{\rm crit}, z_{\rm rei}, V_{\rm crit,r}) = (10^{-3}, 35\,{\rm km\ s^{-1}}, 11, 10\,{\rm km\ s^{-1}})$ compared to the observed distributions of absolute magnitude (left) and stellar velocity dispersions (right). The format of the left panel is the same as Figure 5. The right panel shows predicted and observed velocity dispersions only for the SDSS dwarfs — i.e., those with $M_V > -11$ — with data taken from Simon & Geha (2007).

los with the theoretically predicted $c(M)$ relation have only a weak dependence of M_{300} on total mass over the range $\sim 10^7 - 10^{10} M_\odot$ that hosts observed Milky Way satellites (see Macciò et al. 2009 for further discussion). Thus our models and the models of Macciò et al. (2009) are able to reproduce the narrow observed range of M_{300} without much difficulty (see also Li et al. 2008, who examine M_{600} rather than M_{300}). We note, however, that if we also allow satellites to form stars with efficiency $F_* = 10^{-3}$ before reionization (Model 3A), then the M_{300} range for the lowest luminosity dwarfs, with $M_V > -3$, extends downwards to $M_{300} \sim 10^{6.5} M_\odot$ (blue circles in Figure 13). Thus, careful dynamical measurements for the faintest dwarfs could in principle distinguish whether they arise mainly from pre-reionization star formation or from highly suppressed post-reionization star formation in more massive halos. It is noticeable that our model as well as the models of Macciò et al. (2009) and Li et al. (2008) predicts that M_{300} or M_{600} should slightly increase with galaxy luminosity contradicting the observations, where there is no correlation at all of M_{300} versus luminosity(Strigari et al. 2008). The reason of this disagreement is yet to be understood. It either can be caused by some problems with the data (selection effects or systematics in M_{300} measurements) or by some astrophysical effects. For example Macciò et al. (2009) eliminates the correlation of M_{300} versus luminosity by assuming that the inner profile of the halos with low concentration (i.e. massive halos) is modified during the process of tidal stripping(Kazantzidis et al. 2004).

Comparing the middle and upper panels shows that a small number of objects have $M(z = 0)$ lower than M_{300}, which is possible because we calculate M_{300} based on the sub-halo profile at accretion. The tidal radii of these systems are < 300 pc, but they are all faint satellites for which the stellar Plummer radii are small. While their true M_{300} values should be $M(z = 0)$, the values calculated in the upper panel are probably more directly comparable to the quantities estimated by Strigari et al. (2008), who extrapolate to 300 pc for the faintest systems assuming that they are not tidally truncated within this radius. To minimize the tidal effects one may also compute the masses within 100 pc instead of 300 pc. For our simulated galaxies we also derive M_{100}, which are in the range $1 \times 10^6 - 4 \times 10^6\, M_\odot$ and are also consistent with the $M_{100} \approx 1 \times 10^6 - 3 \times 10^6\, M_\odot$ measurements from Strigari et al. (2008)(supplementary information).

The bottom panel of Fig. 13 shows the value of $M_{\rm sat}$ as a function of luminosity. The relation obviously reflects the underlying formula used to assign stellar masses to the DM halos (eqn. 5), and the scatter caused by the range of accretion redshifts (which affects the $M_{\rm sat} - V_{\rm circ}$ mapping) is small. Even the faintest observable dwarfs have $M_{\rm sat} \sim 10^{8.5} M_\odot$, but they have star formation efficiencies of only $\sim 10^{-5}$. The difference between the middle and bottom panels illustrates the effect of tidal stripping. Nearly all the spread of $M(z = 0)$ at fixed M_V comes from different degree of tidal stripping.

Figure 14 compares the distribution of heliocentric distances of the MW satellites found in the SDSS to the predicted distribution for $M_V > -11$ satellites from our fiducial model. We show one distribution for each of the six Monte Carlo halo realizations. There are significant halo-to-halo variations in the predicted distributions, and the observed distribution follows the lower envelope of the predictions. The distance distribution is strongly influenced by the radial selection effects (the model predictions would be very different if we did not include them), but it also depends on the radial profile of sub-halos and the dependence of this profile on $M_{\rm sat}$ and $z_{\rm sat}$, so match-

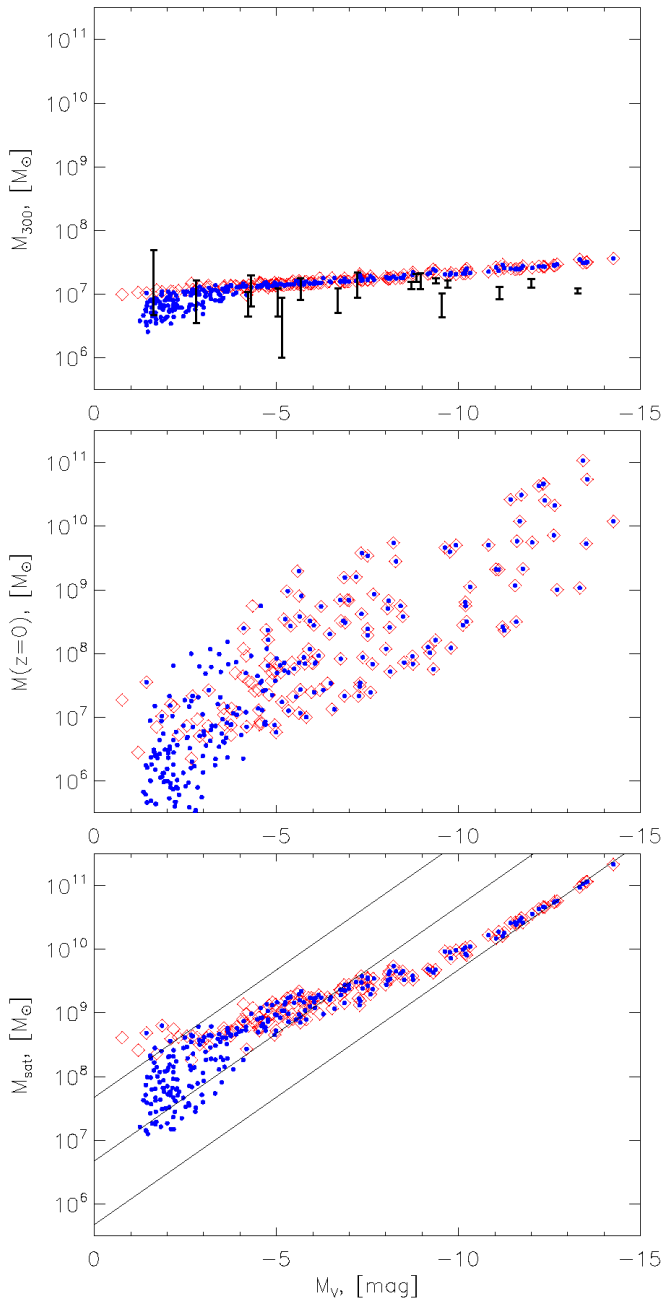

FIG. 13.— Masses of the DM sub-halos within the central 300 pc (top), their total present-day masses (middle) and their masses at the time of accretion into larger halos (bottom). We only show halos hosting observable satellites within the MW virial radius, as a function of satellite luminosity. Red diamonds show all the observable galaxies from six realizations of the fiducial Model 3B with $(F_*, V_{\rm crit}, z_{\rm rei}, V_{\rm crit,r}) = (10^{-3}, 35\,{\rm km\ s^{-1}}, 11, 10\,{\rm km\ s^{-1}})$. Blue filled circles show the predictions of Model 3A, which includes pre-reionization dwarfs (or, equivalently, has $V_{\rm crit,r} = 0$). Error bars show the estimates of M_{300} for observed MW satellites from (Strigari et al. 2008). Solid lines in the bottom panel show, from top to bottom, $M_*/M_{\rm sat} = 10^{-5}$, 10^{-4}, and 10^{-3}. Our models do not incorporate scatter in the concentration-mass relation; adding the theoretically expected scatter would add roughly 0.15 dex of rms scatter to the M_{300} predictions.

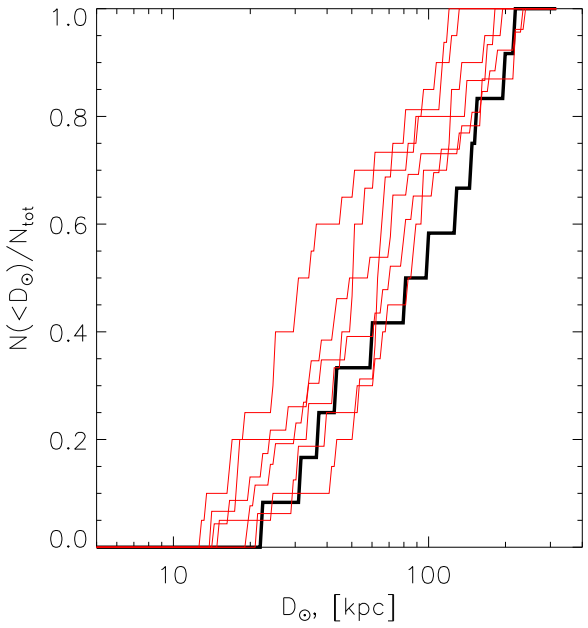

FIG. 14.— Comparison of the model predictions for the cumulative distance distribution of the satellite galaxies with those observed in the SDSS (black line). The predictions of the Model 3B with $(F_*, V_{\rm crit}, z_{\rm rei}, V_{\rm crit,r}) = (10^{-3}, 35\,{\rm km\ s^{-1}}, 11, 10\,{\rm km\ s^{-1}})$ are shown as red lines.

TABLE 2
SATELLITES USED FOR THE ANALYSIS AND PARAMETERS ADOPTED

Galaxy Name	M_V mag	σ_* km/s	$D_\odot$ kpc
Bootes	-6.3	6.6	60
Canes Venatici II	-4.9	4.6	150
Carina	-9.4	6.8	100
Coma	-4.1	4.6	45
Canes Venatici I	-8.6	7.6	220
Draco	-8.75	10.0	80
Fornax	-13.2	10.5	138
Hercules	-6.6	5.1	130
Leo I	-11.5	8.8	250
Leo II	-9.6	6.7	205
Leo IV	-5.0	3.3	160
LMC	-18.6	-	49
Sagittarius	-12.1	11.4	24
Sculptor	-11.1	6.6	80
Sextans	-9.5	6.6	86
Segue 1	-1.5	4.3	23
SMC	-17.2	-	58
Ursa Minor	-9.0	9.3	66
Ursa Major I	-5.5	7.6	100
Ursa Major II	-4.2	6.7	30
Willman I	-2.7	4.3	40

ing the observed distribution is a significant additional success of the model.

5. CONCLUSIONS

The satellite discoveries in the SDSS (Willman et al. 2005; Belokurov et al. 2006, 2007; Zucker et al. 2006; Irwin et al. 2007; Koposov et al. 2007; Walsh et al. 2007) have transformed our understanding of the MW's dwarf satellite population, extending the luminosity range by two orders of magnitude and the implied number of sys-

tems by a factor of 20. Careful quantification of the SDSS satellite detection efficiency (Koposov et al. 2008; Walsh et al. 2008) allows models that specify the relation between dark matter sub-halos and their stellar content to be tested quantitatively against the observations. We have shown that CDM-based models incorporating previously advocated, physically plausible mechanisms for suppressing the stellar content of low mass halos can reproduce the observed properties of the known satellite population, including their numbers, luminosity distribution, stellar velocity dispersions, central masses, and heliocentric radius distribution. However, parameters of these models are tightly constrained, and alternative assumptions lead to conflict with the data. In summarizing our results, it is useful to review both what works and what doesn't.

What works is a model in which the photo-ionizing background suppresses gas accretion onto halos with $V_{\rm circ}(z_{\rm sat}) < V_{\rm crit} \approx 35\,{\rm km\,s^{-1}}$ (Quinn et al. 1996; Thoul & Weinberg 1996; Bullock et al. 2000), with the smooth mass-dependent suppression suggested by numerical simulations (eqn. 5; Gnedin 2000; Hoeft et al. 2006; Okamoto et al. 2008), and inefficient molecular cooling (and/or stellar feedback) drastically reduces the efficiency of star formation in pre-reionization halos below the hydrogen atomic line cooling threshold $V_{\rm crit,r} \approx 10\,{\rm km\,s^{-1}}$ (Haiman et al. 1997; Barkana & Loeb 1999; Machacek et al. 2001; Wise & Abel 2007; O'Shea & Norman 2008; Bovill & Ricotti 2008). There is some degeneracy between this model's two main parameters, $V_{\rm crit}$ and F_*, as shown in Figure 9, but with either parameter fixed the other is fairly well constrained (Figure 8). The other two parameters, $z_{\rm rei}$ and $V_{\rm crit,r}$, just need to be in a range that keeps pre-reionization star formation too low to affect the observable luminosity function. For the values $V_{\rm crit} = 25 - 35\,{\rm km\,s^{-1}}$ favored by numerical simulations, F_* must be $\lesssim 10^{-3}$, so even sub-halos above the $V_{\rm crit}$ threshold have star formation efficiency far lower than the values $F_* \approx 0.1 - 0.4$ found for bright galaxies (e.g., Pizagno et al. 2005; Mandelbaum et al. 2006; Dutton et al. 2007; Gnedin et al. 2007; Xue et al. 2008).

If we assign stellar extents based on observations, and make the reasonable dynamical assumptions discussed in §3.2, then our fiducial model naturally explains the characteristic value and narrow spread of stellar velocity dispersions found for SDSS dwarfs by Simon & Geha (2007). It also explains the characteristic value and narrow range of M_{300} values found by Strigari et al. (2008). The M_{300} values do not depend on the assumed stellar extent, and their narrow range arises from the theoretically predicted structure of CDM halos, which have a weak dependence of M_{300} on total halo mass over the range $M_{\rm halo} \sim 10^8 - 10^{11} M_\odot$. Thus any CDM-based model that prevents formation of observable dwarfs in halos below $\sim 10^7 M_\odot$ should qualitatively reproduce the Strigari et al. (2007, 2008) results (e.g., Li et al. 2008; Macciò et al. 2009). Tempering this success, however, is the fact that the total $z = 0$ sub-halo masses in our model span three orders of magnitude; some of this range is a consequence of tidal stripping, but the span of $M_{\rm sat}$ values is only slightly narrower. The model, in combination with the radial selection biases found by Koposov et al. (2008), also explains the observed heliocentric radius distribution of the SDSS dwarfs, which tests the predicted Galactocentric radius distribution of subhalos and its dependence on mass and accretion redshift.

Many alternative models fail badly in reproducing the observed luminosity distribution. Models with constant $M_*/M_{\rm sat}$ predict far too many faint satellites relative to bright satellites. The SDSS discoveries and luminosity-dependent selection biases do not in themselves resolve the "missing satellite" discrepancy highlighted by Klypin et al. (1999) and Moore et al. (1999); strong mass-dependent suppression of star formation efficiency is still required to reconcile CDM predictions with observations. A simple model in which $M_*/M_{\rm sat} = 10^{-3}(\Omega_b/\Omega_m)(M_{\rm sat}/10^{10}M_\odot)^2$ for $M_{\rm sat} < 10^{10} M_\odot$ is reasonably successful at matching the observations. This successful "empirical" model has a mass dependence of star formation efficiency roughly like that of the successful, physically motivated photo-ionization model (eqn. 5; note that $M_{\rm sat} \propto V_{\rm circ}^3$ at fixed $z_{\rm sat}$).

Models with *sharp* suppression of star formation below the photo-ionization threshold $V_{\rm crit}$ fail at intermediate luminosities, $M_V \sim -8$. Pre-reionization star formation can provide the population of faint dwarfs in such a model, but there is an unacceptable gap between the faint and bright populations (or, for parameter choices that fill the gap, there is an excess of dwarfs at other luminosities). It is striking, therefore, that the *form* of the mass-dependent photo-ionization suppression found in numerical simulations is just that required to match the shape of the observed luminosity distribution. However, the conversion of accreted baryons to stars must be very inefficient for our fiducial model to work, and it is not obvious why this conversion efficiency should be mass independent.

The most interesting of our "negative" conclusions is that star formation in halos before reionization must be extremely inefficient to avoid producing too many satellites in the range $0 \gtrsim M_V \gtrsim -6$. Examination of Figure 8 suggests that the upper limit on the fraction of halo baryons converted to stars is a few $\times 10^{-4}$ for $z_{\rm rei} = 11$, or 10^{-3} if reionization is pushed back to $z_{\rm rei} = 14$. Madau et al. (2008) have reached exactly the same conclusion, with a similar numerical value for the efficiency limit, using the *Via Lactea II* simulation instead of a semi-analytic method to predict the model sub-halo population. Suppression of star formation in halos below the hydrogen atomic line cooling threshold is physically plausible, as the metallicity is low and molecular cooling should be inefficient. For agreement with $N_{\rm obs}(M_V)$, we require pre-reionization suppression in halos with $V_{\rm circ}(z_{\rm rei}) < V_{\rm crit,r} \approx 10\,{\rm km\,s^{-1}}$.

There are several caveats to these conclusions. First, as discussed in §4.2, reproducing the Magellanic Clouds requires that the most massive sub-halos have $M_*/M_{\rm sat} \sim 0.05 - 0.1$, well above the $F_* \sim 10^{-3}$ of our fiducial model. Thus, the photo-ionization suppression described by equation (5) must join onto a continuing increase of star formation efficiency with sub-halo mass above $V_{\rm crit}$, an increase that is presumably driven by other physical mechanisms. Indeed, there is nothing about our results that necessarily picks out photo-ionization as the sup-

pression mechanism in low mass sub-halos, but it is a mechanism that comes in naturally (one might argue inevitably) at the desired scale (Bullock et al. 2000), and the numerically calibrated form yields a good match to the observed luminosity distribution.

In our fiducial model, even the faintest SDSS dwarfs form most of their stars after reionization, but they have $V_{\rm circ}(z_{\rm sat})$ far enough below $V_{\rm crit}$ that their star formation is highly suppressed according to equation (5). The SDSS dwarfs are physically a continuum with the classical dwarfs, and their much lower luminosities are a consequence of the highly non-linear relation between star formation efficiency and halo mass below $V_{\rm crit}$. Halos with $V_{\rm circ}(z_{\rm rei}) > V_{\rm crit,r}$ form pre-reionization stars, but in nearly all cases they grow large enough by $z_{\rm sat}$ that the post-reionization population dominates by a large factor. A small number of systems with $M_V \approx -5$ could have large fractions of pre-reionization stars, but at any luminosity such systems are rare. These conclusions are robust within our framework, but if we allowed for departures from our adopted prescriptions — in particular if photo-ionization suppression for $V_{\rm circ} \ll V_{\rm crit}$ were more aggressive than equation (5) implies and pre-reionization suppression weaker than we have assumed — then it might be possible to construct models in which many dwarfs with $M_V \gtrsim -6$ are pre-reionization "fossils." The efficiency of converting halo baryons to stars in these systems must still be $\sim 10^{-4}$ or less to avoid producing too many faint satellites. Bovill & Ricotti (2008) and Salvadori et al. (2009) have argued that halos cooling by H_2 before reionization naturally give rise to the physical and chemical properties of the SDSS dwarfs. However, even the low star formation efficiencies $\sim 0.5\% - 2\%$ found by Salvadori et al. (2009) appear far too high to be consistent with the observed number counts. On the other hand, Busha et al. (2009) propose a model in which post-reionization suppression of star formation is highly efficient (a sharp threshold) but the star formation efficiency in pre-reionization halos is strongly mass dependent, effectively spreading the low luminosity peak evident in our Figure 6 up towards higher luminosities so that it fills out the entire faint end of the luminosity function.

A third caveat is that we do not explain the origin of the observed stellar extents; we just show that once the observed extents are adopted as inputs, then the observed stellar velocity dispersions emerge naturally. One possible explanation is that the baryons in low mass halos condense *until* they reach a scale at which the velocity dispersion is a few km s^{-1}, and that this minimum dispersion provides the conditions necessary for star formation. We also have not attempted to explain the chemical abundance distributions or star formation histories of the satellites (see, e.g., Orban et al. 2008; Salvadori, Ferrara, & Schneider 2008; Salvadori et al. 2009).

A final caveat is that we have assumed that all dwarfs luminous enough to be found in the SDSS also lie above the surface brightness threshold for detection, which is about 30 mag arcsec^{-2} (Koposov et al. 2008). Since some of the known satellites approach this threshold, it is possible that others fall below it. A large population of lower surface brightness dwarfs would change the number counts that our model reproduces. Note also that a large population of pre-reionization dwarfs would be observationally allowed if they lie below the surface brightness threshold; however, even in this scenario the pre-reionization dwarfs do not account for the presently known satellites. Deeper large area imaging surveys, such as PanSTARRS, the Dark Energy Survey, and LSST, will show whether the MW satellite population includes a significant number of lower surface brightness systems.

Our model makes several predictions that can be tested by these upcoming surveys or by further follow-up studies of known dwarfs. Deeper surveys should reveal many more satellites, more than 200 with $M_V < 0$ and $D_\odot < 400$ kpc over the full sky, with the luminosity function shown in Figure 11. Deep imaging of Andromeda and other nearby galaxies can show whether they have similar satellite systems, though these searches will not reach the extremely low luminosities that can be probed in the MW. Most satellites in our model have stellar extents that are substantially smaller than the present-day tidal radius of their host halo. Tidal tails and tidal disruption should be rare, an implication that may be challenged by photometric evidence on the profiles and shapes of the ultra-faint galaxies, which have been interpreted as signs of tidal distortion or disruption (e.g. Martin et al. 2008). Measurements of the total sub-halo masses of known dwarfs would provide a powerful test of the model predictions in Figure 13, but the small stellar extents may make such measurements impossible. Our models predict that satellites continue to form stars down to $z_{\rm sat}$ or below, and many observable systems should have $z_{\rm sat} = 1 - 2$ (see Figure 2). These predictions may be testable with detailed stellar population modeling.

Our results greatly strengthen the argument (Bullock et al. 2000; Benson et al. 2002; Somerville 2002; Kravtsov et al. 2004) that photo-ionization naturally reconciles the CDM-predicted sub-halo population with the observed dwarf spheroidal population, thus solving the "missing satellite problem" highlighted by Klypin et al. (1999) and Moore et al. (1999). The fiducial model presented here offers a detailed, quantitative resolution of this problem in light of new, greatly improved observational constraints, while relying on previously postulated and physically reasonable mechanisms to suppress star formation in low mass halos. The MW satellites provide a fabulous laboratory for studying galaxy formation at the lowest mass scales, and much remains to be understood about gas cooling, star formation, feedback, and chemical enrichment in these systems. These issues provide challenging targets for numerical simulations and semi-analytic models, whose predictions can be tested against detailed studies of the dynamics and stellar populations of the known dwarf satellites and of the many new satellites that will be revealed by the next generation of sky surveys.

S. K. was supported by the DFG through SFB 439 and by a EARA-EST Marie Curie Visiting fellowship. J. Y. is supported by the Harvard College Observatory under the Donald H. Menzel fund. D. W. acknowledges support from NSF grant AST-0707985 and the hospitality of the Institut d'Astrophysique de Paris during part of

this work. S.K. acknowledges hospitality from the Kavli Institute for Theoretical Physics (KITP) Santa Barbara during the workshop "Building the Milky Way". We thank James Bullock for his helpful comments on the paper and the anonymous referee for prompt review and constructive comments.

This paper relies heavily on data from the Sloan Digital Sky Survey. Funding for the SDSS and SDSS-II was provided by the Alfred P. Sloan Foundation, the Participating Institutions, the National Science Foundation, the U.S. Department of Energy, the National Aeronautics and Space Administration, the Japanese Monbukagakusho, the Max Planck Society, and the Higher Education Funding Council for England. The SDSS was managed by the Astrophysical Research Consortium for the Participating Institutions, which are listed at the SDSS Web Site, `http://www.sdss.org/`.

REFERENCES

Abazajian, K. 2006, Phys. Rev. D, 73, 063513
Adelman-McCarthy, J. K., et al. 2008, ApJS, 175, 297
Barkana, R., & Loeb, A. 1999, ApJ, 523, 54
Belokurov, V., et al. 2006, ApJ, 647, L111
Belokurov, V., et al. 2007, ApJ, 654, 897
Belokurov, V., et al. 2008, ApJ, 686, L83
Benson, A. J., Frenk, C. S., Lacey, C. G., Baugh, C. M., & Cole, S. 2002, MNRAS, 333, 177
Bode, P., Ostriker, J. P., & Turok, N. 2001, ApJ, 556, 93
Bond, J. R., Cole, S., Efstathiou, G., & Kaiser, N. 1991, ApJ, 379, 440
Bovill, M. S., & Ricotti, M. 2008, ArXiv e-prints, 806, arXiv:0806.2340
Bruzual, G., & Charlot, S. 2003, MNRAS, 344, 1000
Bryan, G. L., & Norman, M. L. 1998, ApJ, 495, 80
Bullock, J. S., Kravtsov, A. V., & Weinberg, D. H. 2000, ApJ, 539, 517
Bullock, J. S., Kolatt, T. S., Sigad, Y., Somerville, R. S., Kravtsov, A. V., Klypin, A. A., Primack, J. R., & Dekel, A. 2001, MNRAS, 321, 559
Busha, M. T., Alvarez, M. A., Wechsler, R. H., Abel, T., & Strigari, L. E. 2009, arXiv:0901.3553
Charlot, S., Worthey, G., & Bressan, A. 1996, ApJ, 457, 625
Diemand, J., Kuhlen, M., & Madau, P. 2007, ApJ, 657, 262
Dunkley, J., et al. 2008, ArXiv e-prints, 803, arXiv:0803.0586
Dutton, A. A., van den Bosch, F. C., Dekel, A., & Courteau, S. 2007, ApJ, 654, 27
Eisenstein, D. J., & Hu, W. 1999, ApJ, 511, 5
Fan, X., et al. 2006, AJ, 132, 117
Geha, M., Willman, B., Simon, J. D., Strigari, L. E., Kirby, E. N., Law, D. R., & Strader, J. 2008, arXiv:0809.2781
Gnedin, N. Y. 2000, ApJ, 542, 535
Gnedin, O. Y., Weinberg, D. H., Pizagno, J., Prada, F., & Rix, H.-W. 2007, ApJ, 671, 1115
Irwin, M. J., et al. 2007, ApJ, 656, L13
Jeans, J. H. 1919, Cambridge, University press, 1919
Haiman, Z., Rees, M. J., & Loeb, A. 1997, ApJ, 476, 458
Hoeft, M., Yepes, G., Gottlöber, S., & Springel, V. 2006, MNRAS, 371, 401
Kamionkowski, M., & Liddle, A. R. 2000, Phys Rev Lett, 84, 4525
Kazantzidis, S., Mayer, L., Mastropietro, C., Diemand, J., Stadel, J., & Moore, B. 2004, ApJ, 608, 663
Kauffmann, G., White, S. D. M., & Guiderdoni, B. 1993, MNRAS, 264, 201
Klypin, A., Kravtsov, A. V., Valenzuela, O., & Prada, F. 1999, ApJ, 522, 82
Koposov, S., et al. 2007, ApJ, 669, 337
Koposov, S., et al. 2008, ApJ, 686, 279
Kravtsov, A. V., Gnedin, O. Y., & Klypin, A. A. 2004, ApJ, 609, 482
Li, Y.-S., Helmi, A., De Lucia, G., & Stoehr, F. 2008, arXiv:0810.1297
Macciò, A. V., Dutton, A. A., van den Bosch, F. C., Moore, B., Potter, D., & Stadel, J. 2007, MNRAS, 378, 55
Macciò, A. V., Kang, X., & Moore, B. 2009, ApJ, 692, L109
Machacek, M. E., Bryan, G. L., & Abel, T. 2001, ApJ, 548, 509
Madau, P., Kuhlen, M., Diemand, J., Moore, B., Zemp, M., Potter, D., & Stadel, J. 2008, ApJ, 689, L41
Mandelbaum, R., Seljak, U., Kauffmann, G., Hirata, C. M., & Brinkmann, J. 2006, MNRAS, 368, 715
Martin, N. F., Ibata, R. A., Chapman, S. C., Irwin, M., & Lewis, G. F. 2007, MNRAS, 380, 281
Martin, N. F., de Jong, J. T. A., & Rix, H.-W. 2008, ArXiv e-prints, 805, arXiv:0805.2945
Mateo, M. L. 1998, ARA&A, 36, 435
Moore, B., Ghigna, S., Governato, F., Lake, G., Quinn, T., Stadel, J., & Tozzi, P. 1999, ApJ, 524, L19
Metz, M., & Kroupa, P. 2007, MNRAS, 376, 387
Narayanan, V. K., Spergel, D. N., Davé, R., & Ma, C.-P. 2000, ApJ, 543, L103
Navarro, J. F., Frenk, C. S., & White, S. D. M. 1997, ApJ, 490, 493
Okamoto, T., Gao, L., & Theuns, T. 2008, ArXiv e-prints, 806, arXiv:0806.0378
Orban, C., Gnedin, O. Y., Weisz, D. R., Skillman, E. D., Dolphin, A. E., & Holtzman, J. A. 2008, ArXiv e-prints, 805, arXiv:0805.1058
O'Shea, B. W., & Norman, M. L. 2008, ApJ, 673, 14
Peñarrubia, J., Navarro, J. F., & McConnachie, A. W. 2008, ApJ, 673, 226
Pizagno, J., et al. 2005, ApJ, 633, 844
Plummer, H. C. 1911, MNRAS, 71, 460
Press, W. H., & Schechter, P. 1974, ApJ, 187, 425
Quinn, T., Katz, N., & Efstathiou, G. 1996, MNRAS, 278, L49
Salvadori, S., Ferrara, A., & Schneider, R. 2008, MNRAS, 386, 348
Salvadori, S. & Ferrara, A. 2009, arXiv:0812.3151 McDonald, P., & Trac, H. 2006, Physical Review Letters, 97, 191303
Seljak, U., Makarov, A., McDonald, P., & Trac, H. 2006, Physical Review Letters, 97, 191303
Shaw, L., Weller, J., Ostriker, J. P., & Bode, P. 2006, ApJ, 646, 815
Simha, V., Weinberg, D. H., Dave, R., Gnedin, O. Y., Katz, N., & Keres, D. 2008, arXiv:0809.2999
Simon, J. D., & Geha, M. 2007, ApJ, 670, 313
Somerville, R. S., & Primack, J. R. 1999, MNRAS, 310, 1087
Somerville, R. S. 2002, ApJ, 572, L23
Somerville, R. S., Bullock, J. S., & Livio, M. 2003, ApJ, 593, 616
Spergel, D. N., & Steinhardt, P. J. 2000, Phys Rev Lett, 84, 3760
Spergel, D. N., et al. 2007, ApJS, 170, 377
Strigari, L. E., Bullock, J. S., Kaplinghat, M., Diemand, J., Kuhlen, M., & Madau, P. 2007, ApJ, 669, 676
Strigari, L. E., Bullock, J. S., Kaplinghat, M., Simon, J. D., Geha, M., Willman, B., & Walker, M. G. 2008, Nature, 454, 1096
Stoehr, F., White, S. D. M., Tormen, G., & Springel, V. 2002, MNRAS, 335, L84
Tegmark, M., et al. 2006, PRD, 74, 123507
Tinker, J. L., & Conroy, C. 2008, arXiv:0804.2475
Tollerud, E. J., Bullock, J. S., Strigari, L. E., & Willman, B. 2008, ArXiv e-prints, 806, arXiv:0806.4381
Thoul, A. A., & Weinberg, D. H. 1996, ApJ, 465, 608
van den Bosch, F. C., et al. 2007, MNRAS, 376, 841
Viel, M., Lesgourgues, J., Haehnelt, M. G., Matarrese, S., & Riotto, A. 2005, Phys. Rev. D, 71, 063534
Walker, M. G., Mateo, M., Olszewski, E. W., Gnedin, O. Y., Wang, X., Sen, B., & Woodroofe, M. 2007, ApJ, 667, L53
Walsh, S. M., Jerjen, H., & Willman, B. 2007, ApJ, 662, L83
Walsh, S., Willman, B., & Jerjen, H. 2008, ArXiv e-prints, 807, arXiv:0807.3345
Weinberg, D. H., Hernquist, L., & Katz, N. 1997, ApJ, 477, 8
Weinmann, S. M., Macciò, A. V., Iliev, I. T., Mellema, G., & Moore, B. 2007, MNRAS, 381, 367
Willman, B., Dalcanton, J., Ivezić, Ž., Jackson, T., Lupton, R., Brinkmann, J., Hennessy, G., & Hindsley, R. 2002, AJ, 123, 848
Willman, B., et al. 2005, ApJ, 626, L85

Wilkinson, M. I., Kleyna, J., Evans, N. W., & Gilmore, G. 2002, MNRAS, 330, 778
Wise, J. H., & Abel, T. 2007, ApJ, 671, 1559
Xue, X. -., et al. 2008, ArXiv e-prints, 801, arXiv:0801.1232
York, D. G., et al. 2000, AJ, 120, 1579
Yoo, J., Miralda-Escudé, J., Weinberg, D. H., Zheng, Z., & Morgan, C. W. 2007, ApJ, 652, 26
Zentner, A. R., & Bullock, J. S. 2003, ApJ, 598, 49
Zentner, A. R., Berlind, A. A., Bullock, J. S., Kravtsov, A. V., & Wechsler, R. H. 2005, ApJ, 624, 505
Zucker, D. B., et al. 2006, ApJ, 643, L103